UNIVERSIDADE DE LISBOA
FACULDADE DE CIÊNCIAS
DEPARTAMENTO DE ENGENHARIA GEOGRÁFICA, GEOFÍSICA E ENERGIA

Moisture Transport and Extreme Precipitation Events over the Iberian Peninsula

Tomás Heitor Reis Gaspar

Mestrado em Ciências Geofísicas

Dissertação orientada por:
Professor Doutor Ricardo Machado Trigo
Doutor Alexandre Miguel Urbano Da Fonseca Ramos

2024

Resumo

Palavras chave: Península Ibérica, Extremos de Precipitação acumulada, Classificação Eventos Extremos, Rios Atmosféricos, Transporte de humidade

A Península Ibérica (PI) é caracterizada essencialmente por dois tipos de clima. O clima oceânico, predominante na zona noroeste, é marcado por verões amenos nas regiões costeiras do Atlântico, e o clima mediterrâneo que é caracterizado por uma significativa variabilidade espacial e temporal de temperatura e precipitação (Lionello et al., 2012). Essa variabilidade deve-se principalmente ao fato da PI estar localizada entre duas massas de água contrastantes (Oceano Atlântico e Mar Mediterrâneo) mas também devido à orografia e às trajetórias das tempestades (Martin-Vide and Gil Olcina, 2001). Assim, a Iberia apresenta grande variabilidade sazonal e interanual do seu clima (Ruti et al., 2016). No inverno, o clima é ameno e húmido, dominado principalmente por padrões de larga escala como North Atlantic Oscilation (NAO), Eastern Atlantic (EA), e com frequentes tempestades provenientes do Atlântico, enquanto que o verão é habitualmente quente e seco. Espacialmente, a precipitação concentra-se na costa do Mediterrâneo no outono, o norte e o oeste da PI apresentam um máximo no inverno, e as áreas interiores na primavera (Martin-Vide and Gil Olcina, 2001).
A variabilidade interanual é representada por anos bastante húmidos, como 2001 e 2010 (Vicente-Serrano et al., 2011), intercalados com anos de seca recorde, como os de verão de 2005 e 2012 (García-Herrera et al., 2007; Trigo et al., 2014). A Iberia é considerada um "hot spot" relativamente às mudanças climáticas devido à sua vulnerabilidade a extremos de temperatura (Cardoso et al., 2019), secas (Soares et al., 2017) e impactos relacionados. Nesse contexto, eventos extremos podem ser críticos para os ecossistemas e para as os humanos, pois o aumento das temperaturas devido às alterações climáticas pode agravar ainda mais as secas, ondas de calor e escassez de água. Vários estudos sobre as tendências atuais na precipitação já mostram um aumento no número de eventos extremos de precipitação, ao mesmo tempo que a precipitação anual diminui (De Lima et al., 2013, 2015; Soares et al., 2017). Eventos de precipitação extrema estão bem documentados na PI (Casanueva et al., 2014), frequentemente acompanhados por fortes chuvas, inundações e deslizamentos de terra, impactando significativamente a população local, infraestruturas e economia (Gaspar et al., 2023; Ramos et al., 2014, 2016). Projeções climáticas para o futuro sugerem que as mudanças climáticas podem aumentar a frequência e intensidade desses eventos, especialmente na região oeste (Cardoso Pereira et al., 2019). Vários autores procuram perceber melhor as causas e impactos de eventos extremos de precipitação na Península Ibérica, recorrendo ao registo histórico de precipitação extrema (Ramos et al., 2014, 2016; Vicente-Serrano et al., 2010). Por outro lado, outros trabalhos utilizaram modelos climáticos globais ou regionais e diferentes cenários para estimar mudanças futuras na precipitação extrema sob diferentes cenários climáticos (Soares et al., 2017, 2023). Em geral, nos cenários climáticos futuros, embora seja esperada uma diminuição na quantidade anual de precipitação na maior parte do território, quanto mais intenso for o cenário de emissões, maior será o aumento no número de dias com chuvas intensas, sendo

a região norte mais suscetível a chuvas extremas (Soares et al., 2017).
Dada a importancia em compreender tais mecanismos, principalmente num regime de mudança climática, este estudo focou-se em três tópicos principais:
Em primeiro lugar, classificaram-se eventos extremos de precipitação, com duração variavel, sobre a PI, seguido por uma análise mais detalhada para cada bacia hidrográfica. Essa análise permitiu a identificação de eventos de precipitação extrema, incluindo o episódio de novembro de 1997 no sul de Portugal e Espanha, o evento de março de 2001 no Rio Douro e as inundações de 2008 na região de Lisboa. Foi apresentada uma abordagem sistemática para avaliar períodos de precipitação extrema na região da PI, analisando anomalias de precipitação acumulada em vários intervalos de tempo desde a escala diária à de 10 dias. Eventos persistentes de precipitação podem levar a inundações progressivas de larga escala e movimentos disruptivos de deslizamentos de terra, com impactos socioeconômicos significativos.(Zêzere et al., 2014; Trigo, 2005). Assim, a identificação de extremos de precipitação em diferentes escalas de tempo pode ajudar a entender a possível progressão das inundações. Foi demonstrado que certos eventos extremos com escalas de tempo mais curtas (por exemplo, 1 a 3 dias) podem não aparecer nas principais classificações para escalas de tempo mais longas (por exemplo, 7 a 10 dias). Além disso, certos eventos associados a uma bacia hidrográfica específica podem não estar presentes nas classificações obtidas para as bacias hidrográficas vizinhas, independentemente da escala de tempo considerada.
A magnitude de um episódio de precipitação é determinada considerando a área (em percentagem) que apresenta anomalias de precipitação acima de dois desvios-padrão (STD) e os valores médios dessas anomalias sobre essa área. A metodologia foi aplicada para avaliar períodos de precipitação extrema em toda a PI e em alguns domínios específicos; Portugal e as seis principais bacias hidrográficas da PI (Minho, Douro, Tejo, Guadiana, Guadalquivir e Ebro). Através de vários exemplos representativos, fez-se algumas observações importantes, nomeadamente:

- A metodologia desenvolvida revelou-se útil na identificação de episódios de precipitação extrema nos vários domínios considerados. Uma vez que os eventos extremos mais referidos na literatura ocupam lugares cimeiros nos rankings.
- Os principais episódios de precipitação para as seis diferentes bacias hidrográficas são em grande parte não coincidentes, destacando-se a variabilidade espacial de fenômenos de precipitação extrema na PI.

Ao serem identificados eventos extremos de precipitação, tanto temporalmente como espacialmente, foram criadas bases de dados para diferentes domínios e escalas de tempo e estas são uma mais valia para diferentes estudos que visam compreender as causas e consequências de eventos extremos de precipitação. Isso inclui hidrólogos, gestores de recursos hídricos e seguradoras de atividades socioeconômicas como agricultura e produção de energia hidroelétrica.
O segundo tópico deste trabalho, exposto no capítulo 3 centrou-se nos padrões de transporte de humidade, particularmente nos Rios Atmosféricos (ARs), utilizando um algoritmo de deteção automático de acordo com parâmetros espaciais e temporais específicos em relação aos dados de Transporte integrado de vapor de água (IVT) recorrendo a dados de reanálise (ERA-5). O transporte de humidade dos oceanos para os continentes é um aspeto crucial do ciclo hidrológico atmosférico e representa a principal ligação entre a evaporação oceânica e a precipitação continental (Peixoto and Oort, 1992; Gimeno et al., 2012). Em condições extremas, pode ocorrer transporte anómalo de humidade, resultando frequentemente em eventos extremos de precipitação ao atingir a zona costeira, podendo levar a fortes inundações, com impactos socioeconómicos significativos. Desde que o termo foi adotado há quase três décadas, sabemos

que os ARs correspondem a longos e estreitos corredores de vapor de água que fluem na atmosfera terrestre. Estes fenómenos atmosféricos são responsáveis por transportar grandes quantidades de humidade dos trópicos para as médias latitudes, podendo resultar em eventos significativos de precipitação, inundações e deslizamentos de terra (Gaspar et al., 2023; Liu et al., 2021; Slinskey et al., 2020; Ramos et al., 2016; Ramos et al., 2014; Liberato et al., 2013). O estudo e compreensão dos ARs representa atualmente uma área de interesse crescente entre cientistas, gestores de recursos hidrícos e mesmo do público em geral devido ao seu impacto nos recursos hídricos e em eventos climáticos extremos. Uma análise global recente sobre o papel dos ARs na condução de extremos hidrológicos revelou que estes sistemas têm o potencial de causar não apenas inundações extremas em grandes bacias hidrográficas, mas também a ocorrência de secas quando os ARs estão inativos (Liu et al., 2021). A comunidade científica também desenvolveu métodos para prever a ocorrência de ARs, o que pode melhorar na gestão da água e a prevenção de inundações. Estudos como Liu (2021), Leung (2009) e Wick (2013) foram conduzidos para entender a dinâmica, variabilidade e previsibilidade destes fenómenos. Pesquisas recentes sugerem que a frequência e intensidade dos ARs têm aumentado em algumas regiões do mundo, incluindo a costa oeste da América do Norte e da Europa (Brands et al., 2017; Ralph et al., 2019; Slinskey et al., 2020). Alguns estudos revelaram que as interações entre ARs e o sistema climático são complexas e podem ser influenciadas por vários fatores, como o El Niño-Oscilação Sul (ENSO), a Oscilação de Madden-Julian (MJO) e as mudanças climáticas (Ralph et al., 2020; Ramos et al., 2015).

Assim, ao longo do terceiro capítulo procedeu-se à identificação dos ARs que afetaram a Península Ibérica (PI) para período compreendido entre 1959 a 2022, durante os meses de inverno estendido (Outubro a Março). Para atingir esse objetivo, seguiu-se a mesma abordagem utilizada por Ramos (2015), aplicando um algoritmo de deteção automático de ARs na região oeste da Ibéria, recorrendo a dados de reanálise (ERA-5). Após identificar os ARs e analisar as suas características, como comprimento, duração e intensidade, avaliou-se a magnitude da correlação entre a ocorrência de ARs e padrões de circulação atmosférica em larga escala, como a Oscilação do Atlântico Norte (NAO) ou do Atlântico Leste (EA). Os resultados indicam que ocorrem, por ano, uma média de 6 ARs. O número de ARs por mês diminui nos meses após dezembro, com 85 ARs detectados durante esse mês. A maioria dos ARs (190, 52,5%) durou menos de 24 horas, e o seu comprimento variou entre 2040 e 3360 km. Nos passos temporais em que existe a ocorrência de ARs, foram observadas anomalias negativas de pressão do nível do mar (SLP) em torno da Irlanda, enquanto anomalias positivas estavam presentes sobre o norte da África. Essa configuração de gradiente meridional de SLP facilita o transporte de humidade em direção à Península Ibérica, estando intimamente associada aos ARs.

No último tópico deste estudo, abordado no capítulo 4, quantifica-se em que medida grandes quantidades de precipitação estão associadas à presença (ausência) de ARs na região do Atlântico Norte durante o período de 1959 a 2015, comum a ambas as bases de dados (Precipitação e Reanálise). Para atingir este objetivo, os ARs foram classificados em diferentes categorias baseadas no trabalho de Ralph (2019). Os ARs foram classificados com base no valor médio de IVT ao longo do núcleo do AR e respetiva duração do evento. Consequentemente, estabeleceu-se uma relação entre a categoria atribuída ao rio atmosférico e a respetiva magnitude do evento de precipitação extrema. É importante enfatizar uma vez mais que, estando o conjunto de dados de precipitação disponível apenas para o período de 1950 a 2015, a associação entre os dias de precipitação extrema e os ARs será restrita ao período comum (1959-2015).

Os resultados obtidos estão de acordo com a literatura, onde é referida uma uma ligação entre a passagem de ARs e eventos extremos de precipitação (Gaspar et al., 2023; Ramos et al., 2014; Lavers and Villarini, 2013). Com estes resultados, podemos avaliar essa relação tanto quantitativa como qualitativamente sobre a PI tendo por base o conjunto de dados mais recente até à data de realização deste estudo.

Em jeito de conclusão, com elaboração deste trabalho obtem-se um vasto leque resultados:

- Criou-se um banco de dados abrangente de eventos de precipitação extrema para a Península Ibérica (PI), abrangendo vários períodos (1 a 10 dias) de 1950 a 2015. Eventos de precipitação extrema foram estudados para toda a Península Ibérica, Portugal e principais bacias hidrográficas regionais, com foco no período de inverno estendido (Outubro a Março). A análise revela que certos eventos extremos de curto prazo podem não ocupar posições elevadas em escalas de tempo mais longas, e eventos destacados numa determinada bacia hidrográfica podem não aparecer nas classificações das bacias vizinhas, independentemente do período considerado. É importante destacar que os resultados são puramente baseados em estimativas estatísticas e não incluem uma avaliação dos mecanismos físicos por trás desses episódios extremos.

- Identificou-se os ARs que afetaram a PI no período compreendido entre 1959 a 2022. Para o efeito, segue-se a mesma abordagem de Ramos (2015), aplicando um algoritmo objetivo de detecção de ARs na costa oeste da PI recorrendo a dados de reanálise (ERA-5). Após identificar os ARs e analisar as suas características, como comprimento, duração e intensidade, foram estudados os padrões de circulação associados a esses eventos.

- Avaliou-se o impacto dos ARs nos eventos de precipitação extrema. Os eventos de ARs são categorizados com base no trabalho de Ralph (2019). Estabeleceu-se uma relação entre as categorias de AR e a magnitude dos eventos de precipitação extrema associados. Com este trabalho esta relação foi avaliada quantitivamente e qualitativamente recorrendo ao conjunto de dados mais recente disponível até à data.

O estudo conclui que a ocorrência de ARs têm uma contribuição significativa para eventos extremos de precipitação na PI, e o seu impacto potencial deve ser considerado ao avaliar e gerir os riscos associados a esses eventos. Os resultados também destacam a importância de analisar os diferentes subdomínios e escalas de tempo de forma a obter uma melhor compreensão da variabilidade espacial e temporal de eventos extremos de precipitação associados à passagem de ARs. É importante ter presente que estes métodos podem ser reproduzidos para qualquer região afetada por ARs e com dados de precipitação de alta resolução disponíveis (e.g. Chile, Africa do Sul).

Abstract

Keywords: Iberian Peninsula, accumulated precipitation, atmospheric rivers, ranking events, high-resolution dataset

Atmospheric rivers (ARs) are responsible for over 90% of poleward water vapor transport in the mid-latitudes and can produce extreme precipitation when making landfall. Conclusions about anomalous moisture transport patterns and their contribution to extreme precipitation events (EPEs) over the Iberian Peninsula were achieved.

First, the precipitation data is analyzed to obtain a ranking of multi-day extreme precipitation events over the Iberian Peninsula, followed by a more detailed analysis of each river basin. This analysis allowed for the identification of extreme precipitation events, including the November 1997 event in southern Portugal and Spain, the March 2001 episode in River Douro, and the urban floods of 2008 over the Lisbon region.

The second division focused on moisture transport patterns, anomalous moisture transport, and ARs occurrence, using an automated detection algorithm according to specific spatial and temporal parameters relative to the integrated vapor transport (IVT) data from 1959-2022 provided by ERA-5 reanalysis. After identifying ARs and analyzing their characteristics, such as length, duration, and intensity, the study focused on circulation patterns associated with these events. Results demonstrate a strong and positive correlation for the East Atlantic (EA) and a negative correlation for the North Atlantic Oscillation (NAO) Quantification of the relationship between ARs and extreme precipitation events was achieved. ARs were classified by categories and associated with EPs magnitudes and, it can be concluded that the most intense ARs cause the most extreme precipitation events. The study further revealed that, sometimes a stronger AR has less impact on precipitation than a weaker one because it didn't landfall at all or simply had a quick pass by the Iberian Peninsula.

A strong correlation was identified between the occurrence of ARs and extreme precipitation events in the Iberian Peninsula, particularly the most severe events. This correlation was observed in both qualitative and quantitative terms, indicating a clear match between the two phenomena. It is important to keep in mind that these findings could be replicated in other locations with comparable datasets and methodologies. The study highlights the importance of understanding the contribution of ARs to extreme precipitation events and its implications for managing the risks associated with these events in the region.

Acknowledgments

I am reaching out to express my deepest gratitude to Professor Ricardo Trigo for your unwavering support and guidance throughout the process of completing my master's thesis. Your expertise in the field and dedication to fostering a positive learning environment have significantly influenced my research. The insightful feedback and constructive criticism provided by you have not only enhanced the quality of my thesis but have also instilled confidence in my academic capabilities. Your mentorship has been instrumental in shaping my academic journey. I am particularly thankful for the trust you have placed in my abilities.

Supervised by Alexandre Ramos, I am grateful for your continuous support and guidance throughout this academic endeavor. Your commitment to excellence and willingness to share your knowledge have played a crucial role in the successful completion of my thesis

In addition, special acknowledgment is extended to Instituto Português do Mar e da Atmosfera (IPMA). Gratitude is particularly owed to colleague Ricardo Deus for the invaluable provision of data on extreme precipitation during the December 2022 event, significantly enhancing the depth of analysis in this master's thesis.

I would also like to extend my sincere thanks to my colleagues in the faculty department. Your collaboration and camaraderie have enriched my learning experience, and I am grateful for the collective efforts that have contributed to the success of my thesis.

To all the teachers I have had during my university years, thank you for imparting your knowledge and expertise. Each of you has played a vital role in my academic development, and I am truly appreciative of the dedication you have shown to your students.

Last but certainly not least, my heartfelt thanks go to my family. Your unwavering support, encouragement, and understanding have been my pillars of strength. This achievement is as much yours as it is mine, and I am grateful for the love and support that has fueled my academic pursuits.

I feel fortunate to have had such a supportive network, and I look forward to applying the knowledge and skills I have gained in my future endeavours.

This work was supported by a grant through project AMOTHEC (https://doi.org/10.54499/DRI/India/0098/2020) supported by the Portuguese Fundação para a Ciência e Tecnologia (FCT) I.P./MCTES.

Index

List of Figures

List of Tables

Chapter 1

Introduction

The Iberian Peninsula (IP) is characterized by two main climate types. The oceanic climate is marked by temperate summer over the Atlantic coastal regions, and the Mediterranean climate is characterized by significant spatial and temporal variability of temperatures and precipitation (Lionello et al., 2012). This variability is mainly due to the fact the IP is located between two contrasting water masses (the Atlantic Ocean and the Mediterranean Sea), the orography or the storm tracks (Martin-Vide and Gil Olcina, 2001). Iberia exhibits large seasonal and inter-annual variability (Ruti et al., 2016). In winter, the climate is mild and wet, mainly dominated by several teleconnections patterns like the NAO, the East Atlantic patterns and other westward storms originating over the Atlantic, while the summer is hot and dry. Spatially, the precipitation is concentrated on the Mediterranean coast in autumn, the north and west of the IP present a maximum in winter, and the inland areas in spring (Martin-Vide and Gil Olcina, 2001). Inter-annual variability is strong and well represented by wet years such as 2001 and 2010 (Vicente-Serrano et al., 2011), interspersed with record drought years such as those of summer 2005 and 2012 (García-Herrera et al., 2007; Trigo et al., 2014). Iberia is considered a climate change hotspot due to its vulnerability to temperature extremes (Cardoso et al., 2019), droughts (Soares et al., 2017), and related impacts. In this context, extreme events may be critical for human activities, where increased temperatures due to global warming may further exacerbate droughts, heat waves and water shortages as well as more frequent floods. Several studies of current trends in precipitation already show an increase in the number of extreme precipitation events, while the annual precipitation decreases (De Lima et al., 2013, 2015). Extreme precipitation events are well-documented over the Iberian Peninsula (Casanueva et al., 2014), usually accompanied by heavy rainfall, flooding and landslides, significantly impacting the local population, infrastructure, and economy (Ramos et al., 2016). Future climate projections suggest that climate change may increase the frequency and intensity of these events, particularly in the western region (Cardoso Pereira et al., 2019). Several researchers have conducted studies to better understand the causes and impacts of extreme precipitation events over the Iberian Peninsula, focusing on the historical record of extreme precipitation (Vicente-Serrano et al., 2010). In contrast, others have used global or regional climate models and different scenarios to estimate future changes in extreme precipitation under different climate scenarios(Soares et al., 2017). In future climate scenarios, although a decrease in the annual amount over most of the territory is expected, the larger the emissions scenario, the larger the augments of days with strong rainfall, being the northern region more susceptible to extreme rainfall (Soares et al., 2017).

To mitigate extreme events is necessary to know the main drivers that cause them. One of the key players for the extreme precipitation in western Iberia is the Atmospheric Rivers (Ramos et al., 2015; Brands et al., 2017). The term atmospheric rivers (ARs) describes long, narrow corridors of water vapour that

1. INTRODUCTION

are typically associated with a low-level jet stream ahead of the cold front of an extratropical cyclone, exhibiting a river-like appearance when viewed from a bird's-eye perspective (Figure 1.1). These formations are characterized by robust low-level winds and intense moisture transport, spanning vast distances (Newell et al., 1992; Eiras-Barca et al., 2018). The water vapour essential for their construction may originate from evapotranspiration in a distant source region, followed by intense transport covering thousands of kilometres (Knippertz and Wernli, 2010; Garaboa-Paz et al., 2015), or through a small-scale moisture recycling process (Bao et al., 2006). These features are linked to the development of midlatitude/extratropical cyclones, often associated with large-scale dynamics, and are more prevalent during the winter months (Gimeno et al., 2014). The transport of moisture from oceans to continents is a crucial aspect of the atmospheric branch of the water cycle and represents the principal connection between oceanic evaporation and continental precipitation (Peixoto and Oort, 1992; Gimeno et al., 2012). Under extreme conditions, anomalous moisture transport can take place, resulting in extreme precipitation events upon landfall, leading to devastating floods with significant socio-economic impacts (Ramos et al., 2015; Slinskey et al., 2020).

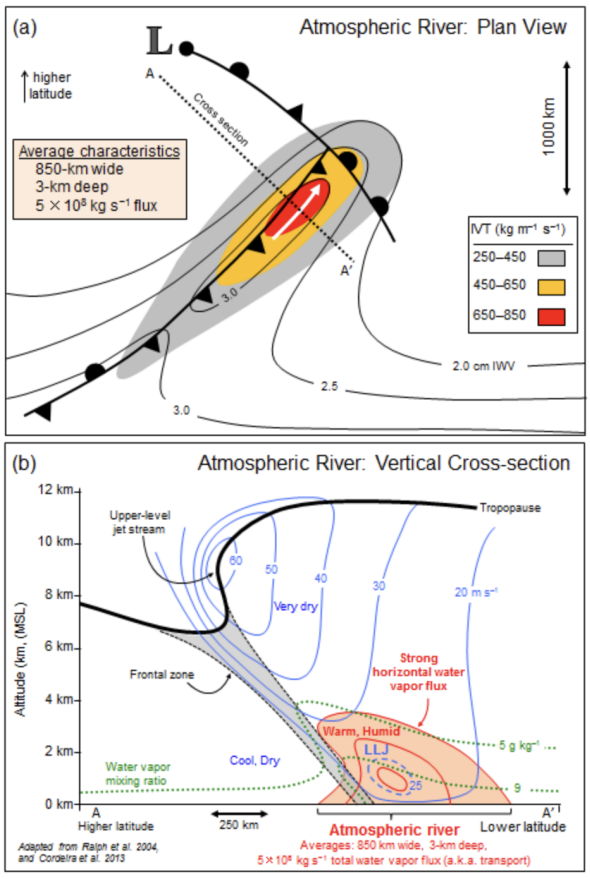

Figure 1.1: Schematic summary of the structure and strength of an atmospheric river based on dropsonde measurements deployed from research aircraft across many atmospheric rivers and on corresponding reanalyses that provide the plan-view context. Magnitudes of variables represent an average midlatitude atmospheric river. (a) Plan view including parent low pressure system and associated cold, warm, and warm-occluded surface fronts. IVT is shown by color fill (magnitude; $\mathrm{kg\,m^{-1}\,s^{-1}}$) and direction in the core (white arrow). Vertically integrated water vapor (IWV; cm) is contoured. A representative length scale is shown. The position of the cross section shown in (b) is denoted by the dashed line A–A′. (b) Vertical cross-section perspective, including the core of the water vapor transport in the atmospheric river (orange contours and color fill) and the pre-cold-frontal low-level jet (LLJ), in the context of the jet-front system and tropopause. Water vapor mixing ratio (green dotted lines; $\mathrm{g\,kg^{-1}}$) and cross-section-normal isotachs (blue contours; $\mathrm{m\,s^{-1}}$) are shown. [Graphic is from American Meteorological Society (2017).

ARs have become an area of increasing interest among scientists, policymakers, and the public due to their impact on water resources, climate variability, and extreme weather events. A recent global analysis conducted on the role of ARs in driving hydrological extremes has revealed that ARs have the potential to cause not only extreme floods in many major drainage basins but also drought occurrence when ARs are inactive (Liu et al., 2021). Researchers have also developed methods for predicting ARs, which can improve water management and flood preparedness. Therefore, studies such as Liu (2021), Leung (2009), and Wick (2013) have been conducted to understand the dynamics, variability, and predictability of these phenomena. Recent research has suggested that the frequency and intensity of ARs have increased in some regions of the world, including the western coast of North America and Europe. Other studies have revealed the complex interactions between ARs and the climate system, which can be influenced by various factors such as the El Niño-Southern Oscillation (ENSO), the Madden-Julian Oscillation (MJO), and climate change (Ramos et al., 2015; Ralph et al., 2020).
Given the importance of the ARs in the extreme precipitation in the Iberian peninsula, the objectives of this work are:

- This study's primary goal is to create a comprehensive database of extreme precipitation events for the Iberian Peninsula, covering various time scales (1 to 10 days) from 1950 to 2015. Utilizing two precipitation datasets (Iberia 01 and Iberia 02) and adopting the methodology from Ramos (2016), the analyses develops objective rankings for extreme precipitation events throughout the entire Iberian Peninsula, Portugal, and major regional river basins, focusing on the extended winter season (October to March). The analysis reveals that certain short-term extreme events may not rank high in longer time scales, and top events in one river basin may not appear in neighboring basins' rankings, irrespective of the time frame. It is important to highlight that the results are purely based on statistical estimation and lack an assessment of the physical mechanisms behind these extreme episodes.

- The second objective of the work is to identify the ARs that affected the IP over the 1959–2022 period during the extended winter months. To achieve this, the same approach as Ramos (2015) is followed, applying an automated ARs detection algorithm to western Iberia using ERA-5 reanalysis datasets (as explained in detail in section 3.1). After identifying ARs and analyzing their characteristics such as length, duration, and intensity, the focus is on circulation patterns associated with these events.

- The investigation focuses on assessing the impact of Atmospheric Rivers (ARs) on extreme precipitation events. AR events are categorized based on Ralph's (2019) work, detailed in section 4.1. The study evaluates the appropriateness of the classification scale by establishing a link between AR categories and the magnitude of associated precipitation extremes. Existing literature suggests a connection between AR landfall and extreme precipitation events (Gaspar et al., 2023; Ramos et al., 2015; Lavers and Villarini, 2013; Ralph et al., 2019), and the current study aims to quantitatively and qualitatively evaluate this relationship over the Iberian Peninsula using the latest dataset available.

Chapter 2

Ranking of Multi-day Extreme Precipitation Events over Iberia

2.1 Datasets and methodology

2.1.1 Precipitation dataset

The main focus in this chapter is on the application of different methods to a good quality precipitation dataset aiming to obtain a ranking of multi-day extreme precipitation events over the Iberian Peninsula. This will be performed through the application of the methodology developed in Ramos's work (2014; 2016). For that, a similar approach to those seminal works was used here, based on two high-resolution regular grid datasets available for all of the Iberian Peninsula (IB01 and IB02). Historically IB02 database was developed first and consists of the merger of two precipitation datasets developed independently for Portugal (PT02, Belo-Pereira et al., 2011) and Spain (SPAIN02, Herrera et al., 2010), which have been developed independently, albeit employing very similar methodologies. The IB02 dataset is defined between 1950-2008 with a resolution of 0.2º latitude-longitude grid, as the name indicates. The IB02 dataset was used recently by different authors, including the analysis of the dynamic mechanisms causing extreme precipitation hazardous events (Liberato et al., 2013; Trigo et al., 2014), the assessment of daily precipitation ranking days in Iberian Peninsula (IP) (Ramos et al., 2015), the role of atmospheric rivers (ARs) in the occurrence of the most anomalous precipitation days (Ramos et al., 2015) or the relationship between the spatial and temporal variability of precipitation and circulation weather types (Ramos et al., 2014). Recently this gridded dataset was upgraded evolving to the IB01 dataset (Herrera et al., 2019) that spans the 1971-2015 period with a 0.1º latitude-longitude grid. Both these datasets are based on a dense network of rain gauges that are all quality-controlled and homogenized (Ramos et al., 2016). Therefore, aiming to work with the greatest temporal extension and the best spatial resolution possible the two datasets were here combined, with 1950-1970 period based on IB02 and for the period between 1971-2015 based on IB01. To achieve consistency in terms of spatial resolution IB02 dataset was artificially upscaled from 0.2º to 0.1º latitude-longitude grid.

2.1.2 Ranking of multi-day extreme precipitation events

In order to obtain the different rankings of precipitation extremes over multi-day accumulated periods a three-step method was applied (Ramos et al., 2016). The first step consists in computing the daily normalized precipitation anomalies (N) given by equation (2.1):

$$N_{c,i,j} = \frac{Precip_{c,i,j} - \mu_{c,i,j}}{\sigma_{c,i,j}} \tag{2.1}$$

Where Precip is the precipitation value for a particular year and day (c) and for a particular grid point (i,j), μ is the daily mean climatological value for that grid point (i,j) and for that particular Julian day (c), and σ is the daily standart desviation (STD) from this Julian Climatologic daily mean (c) also for the grid point (i,j). Only grid points with daily precipitation above 1 mm (wet days) were considered for the climatological computation. Daily Julian mean and STD were computed for the entire dataset period between 1950-2015 (65 years). A 7-day running mean is then applied to the climatological series to smooth the noisy nature of these time series (Ramos et al., 2016). Therefore, the daily normalized precipitation anomalies (N) are computed for each day and grid point.
The second step was applied to obtain accumulated precipitation anomalies for a certain period (p). Since the daily precipitation anomalies were computed in the previous step (Equation (2.1)) and are normalized, the sum of the normalized anomalies over multi-day periods (n) represents the accumulated precipitation anomalies (Equation (2.2)).

$$NCC_{p,i,j} = \sum_{c=1}^{n} N_{c,i,j} \tag{2.2}$$

The final step was to quantify the level of extreme precipitation, proceeding with the computation of the magnitude for each different accumulated precipitation anomaly period. For that it was applied the same procedure developed by Ramos (2016), i.e the magnitude of an extreme (R_M) is given daily by an index that is obtained after multiplying:

- The area (A), in percentage, that has precipitation anomalies (over each accumulated period) above two STD by;
- The mean value of these anomalies (hereafter M) for all grid points that have precipitation anomalies above two STD;
- The magnitude is than given by R_M = A*M

A detailed analysis was performed for eight different spatial domains of the IP, including the most important river basins: (1) Minho, (2) Duero, (3) Tagus, (4) Guadiana, (5) Guadalquivir and (6) Ebro); and additionally, the areas of Portugal and the entire IP. For all these domains the multi-day precipitation rankings (3, 5, 7 and 10 days) were computed, resulting in a total of 32 different rankings (Ramos et al., 2016).
In the forthcoming section, several examples of distinct rankings will be presented, followed by a comprehensive analysis to provide an in depth understanding of the potential usefulness of this analysis. It is noteworthy, however, that the computation of precipitation extremes' magnitudes is independent from the occurrence of significant socioeconomic impacts that may arise. It should be acknowledged, though, that such a relationship could exist in certain circumstances.

2.2 Iberian Peninsula and Portugal

In this section, the ranking results for the entire IP and Portugal will be presented and discussed in detail. Some examples of the top ten events for the different accumulation periods will be presented to give a general idea of how the multi-day ranking analysis works for both domains. In Table 2.1 the top ten cases of the rankings of precipitation extremes for different accumulated periods (3, 5, 7 and 10 days) are shown for: the IP (Table 2.1a), and for Portugal (Table 2.1b). As expected, some results perfectly match the results obtained in Ramos's (2016) work. However, in several occasions while it was possible to identify the same event, there was no perfect match for the ranking position. For example, for the 3-day accumulated period for Iberian Peninsula the November 7 1982 event appears in the fourth position, although it occupies the third position on Ramos (2016) work. Considering that this analysis considers a slightly different dataset, then small differences when comparing to Ramos's (2016) work are expected since these results span more years (1950-2015) as a consequence of including the IB01 dataset.

It can be observed that some of the top positions appear in both tables but in different positions. For instance, if the top event for IP over a 3-day accumulated period (3 March 2001) is considered, the same event over Portugal occupies a lower position (#7; Table 2.1). Conversely, the top event for Portugal for the 3-day accumulated period (14 March 1969) holds position #3 when considering all IP territory (Table 2.1). Ramos (2016) also identified 3 March 2001 as the top event over the Iberian Peninsula

Table 2.1: The ten most anomalous precipitation events in the (a) Iberian Peninsula and (b) Portugal regarding the different accumulated periods (3, 5, 7, and 10 days)

(a) Iberian Peninsula				
Number of Ranking	3 days	5 days	7 days	10 days
1	3 March 2001	16 March 1969	18 March 1969	11 January 1970
2	8 November 1982	30 December 1981	17 March 1969	12 January 1970
3	14 March 1969	31 March 1952	10 February 1979	3 March 1978
4	7 November 1982	5 March 2001	2 March 1978	13 February 1979
5	29 December 1981	8 November 1951	16 March 1969	10 February 1979
6	21 March 1953	4 March 2001	1 March 1978	11 February 1979
7	30 December 1981	31 December 1981	7 March 2001	12 February 1979
8	31 March 1952	15 March 1969	3 March 1978	4 March 1978
9	22 March 1953	10 February 1979	11 February 1979	31 December 1995
10	10 February 1979	28 February 1978	28 February 1978	14 February 1979
(b) Portugal				
Number of Ranking	3 days	5 days	7 days	10 days
1	14 March 1969	16 March 1969	18 March 1969	20 February 1966
2	2 February 1972	31 March 1952	17 March 1969	21 February 1966
3	20 February 1966	15 March 1969	16 March 1969	13 February 1979
4	19 February 1966	21 February 1966	21 February 1966	12 February 1979
5	13 March 1969	8 November 1951	23 March 1956	21 March 1969
6	10 February 1979	4 February 1972	10 February 1979	13 February 1979
7	3 March 2001	10 February 1979	12 February 1979	18 March 1969
8	23 March 1956	19 February 1966	20 February 1966	20 March 1969
9	24 March 1956	30 December 1981	11 February 1979	26 March 1956
10	12 October 1953	24 March 1956	14 February 1979	19 February 1966

for the 3-day accumulated period. Comparing Figure A.1 of the supplementary material with the ones present in Ramos's (2016) work, the overall results are quite similar, as expected. Therefore, a detailed analysis focused on February 1979 was chosen, since several events from 10 to 14 February 1979, are present across almost all the accumulated period rankings in Table 2.1.

Regarding the 3-day accumulation period, 10 February 1979 holds the #6 position for Portugal and the #10 position for the IP. However, for the 10-day accumulation period, five out of the top ten positions (50% of the top ten for 10 days accumulation period over IP) correspond to cases spanning between 10 to 14 February 1979. As mentioned before, the 3-day accumulation period for the event on 10 February 1979 refers to the accumulated normalized precipitation anomalies between 8 and 10 February 1979 and the associated daily precipitation for the three considered days.

As expected a multi-day top position depends on the existence of an event that is characterised by a successive daily ranking anomalous precipitation, that once accumulated during a given period, origins a multi-day top position. Figure 2.1a corresponds to a 3-day accumulated period on 10 February 1979. Thus, regarding the daily IP ranking, 8 February (Figure 2.2a) corresponds to the daily magnitudes of 38.5 (#386), 67.84 for 9 February (#105) (Figure 2.2b) and 126.14 (#12) on the 10 February (Figure 2.2c). During these 3 days, anomalous precipitation above 2 STD, up to 4 STD, was recorded essentially over central and northern Portugal (08 February, Figure 2.2a), reaching Spain in the following 24 hours (Figure 2.2b,c). This sequence produces an accumulated 3-day period on 10 February (Figure 2.1a) with totals of 200 mm recorded over Gêres Natural Park, with accumulation anomalies reaching magnitudes above 10 STD over Lisbon. It is important to note that a larger standardised anomaly (measured in STD may not necessarily correspond to the same area of the maximum total precipitation. Figure 2.1a shows this: Even though, the region with the highest accumulated precipitation values (>160mm) is in the natural park of Gêres, it is in the metropolitan region of Lisbon, where precipitation values are around 100mm, that the standardised anomaly values are more pronounced, reaching up to 10 STD from the climatological mean for that day in this region.

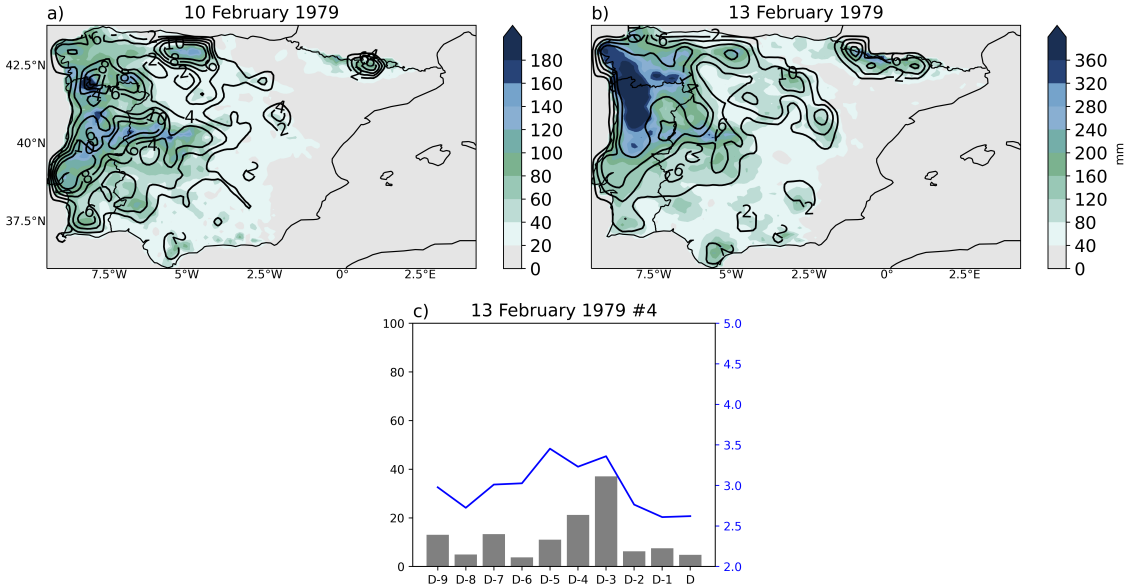

Figure 2.1: (a) Three-day accumulated precipitation (mm, shaded) and corresponding standard deviation anomalies (black contour) for the case in the Iberian Peninsula on 10 February 1979; (b) 10 days accumulated precipitation (mm, shaded) and corresponding standard deviation anomalies (black contour) of the #3 (10 days ranking) case in Iberian Peninsula – 13 February 1979; (c) The percentage of area with anomalies above the 2 STD limit (bars) and the corresponding mean anomalous values (blue line) between 4 February and 13 February 1979 is also shown for the Iberian Peninsula domain.

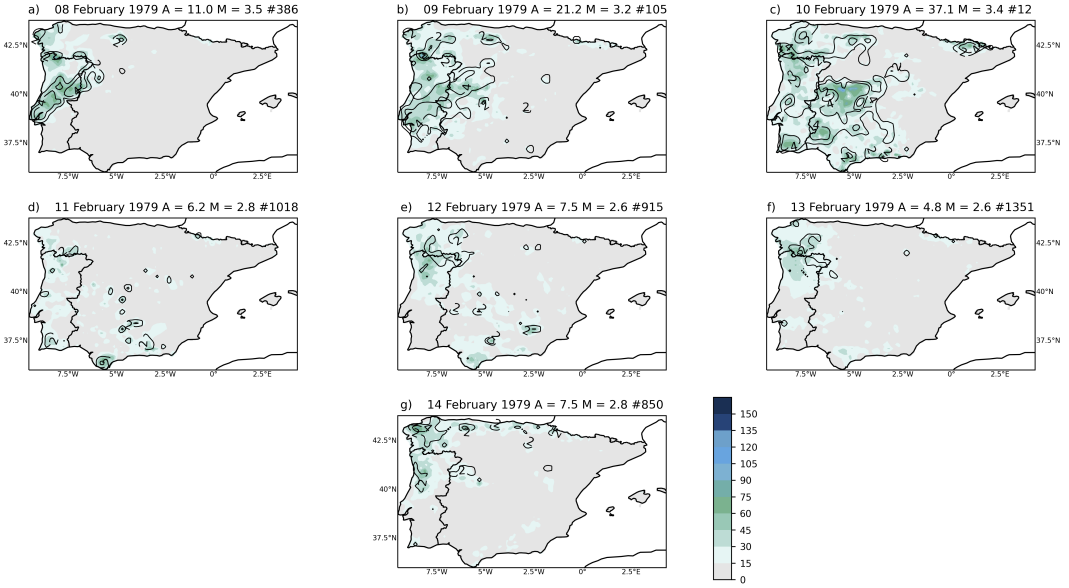

Figure 2.2: Daily precipitation (mm, shaded) and corresponding standard deviation anomalies (black contour) for (a) 8 February 1979, (b) 9 February 1979, (c) 10 February 1979, (d) 11 February 1979, (e) 12 February 1979, (f) 13 February 1979 and (g) 14 February 1979. The standard deviation anomalies were smoothed with the neighbour grid points. Each panel shows the respective date, the area (A), the mean value (M), and the rank position (#) for the individual daily ranking.

The accumulated precipitation anomalies for the 3 days above 2 STD correspond to a total affected area A = 54.67% of the IP with a mean value of these anomalies corresponding to M = 6.43 STD resulting on a magnitude of $RM = A \times M = 351.36$ (Figure 2.1a). Moreover, when examining Table 2.1a, it can be observed that although the 10 February 1979 event only holds the tenth position in the 3-day accumulated precipitation ranking, it reaches higher positions in the 7 and 10-day accumulated precipitation rankings (#3 and #5, respectively). The explanation for these differences is quite simple, in many cases, a particular period may be exceptional at one specific temporal scale but would only be mildly relevant in another multi-day ranking period Ramos et al., 2016. The daily precipitation for IP during the 10-day period (4–13 February 1979) is shown in Figure 2.1c, where it can be noticed that the anomalous precipitation mean stands above 2.5 STD on all days (blue line). From 8 to 10 February, a significant increase in the affected area that is above 2 STD (grey bars) is clearly evident, and on the 10 it reaches the maximum value of 37.1% of all Iberian Peninsula (Figure 2.1c and Figure 2.2). On the 10th of February, the area of precipitation which exceeds 2 STD was found to be dispersed across almost all domains of the IP (Figure 2.2c). The precipitation observed during the last four days (11 to 14) was characterized by lower intensity and more localized distribution, as depicted in Figure 2.2d, e, f, g.

In Figure 2.3, the magnitudes of the top 100 cases for each different anomalous accumulated precipitation ranking are represented, and evidence of a logarithmic decay behaviour on precipitation extremes magnitude on all accumulated periods is clearly seen. Results at the left side of the vertical grey line (representing to the ten most significant cases) correspond to all the magnitude values of the anomalous cases shown in Table 2.1. In Figure 2.3, the differences between the most extreme cases in the IP among the multi-day rankings can be identified. As the period of multi-day rankings increases, an increase in the magnitude values (with the highest values corresponding to the 10-day period) can be observed. This is simply due to the increase in the number of precipitation days included in the accumulation period. Overall, these results are similar to those presented by Ramos (2016). The same results for the other domains were quite similar to the ones presented in Figure 2.3. The average value for the first 100 cases

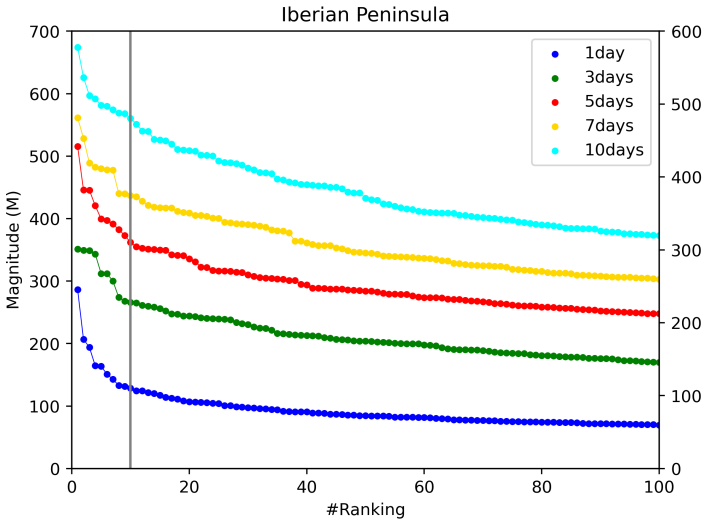

Figure 2.3: The top 100 events magnitude values for each different anomalous accumulated precipitation rankings, 1 day (blue), 3 days (green), 5 days (red), 7 days (orange), and 10 days (light blue), for the Iberian Peninsula. The top ten cases are highlighted, falling to the left of the grey vertical line.

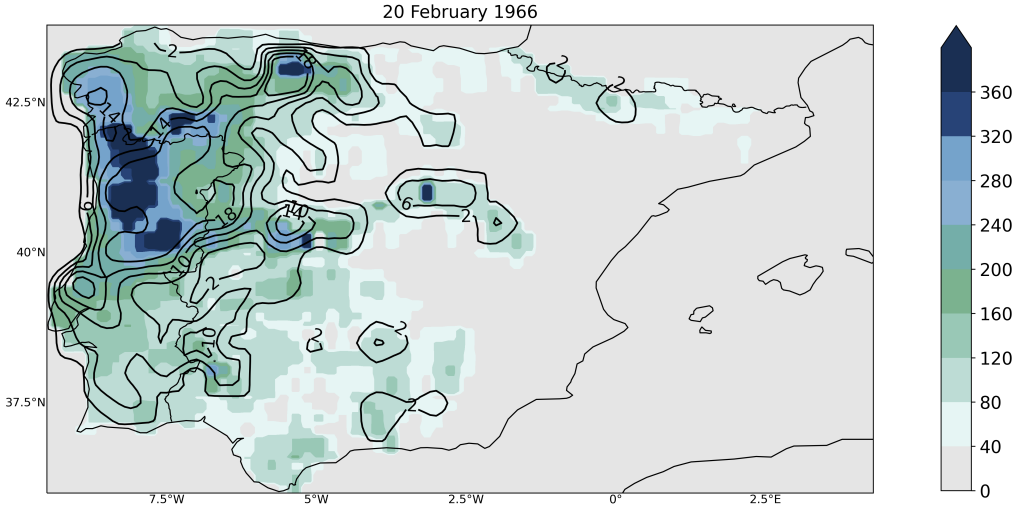

Figure 2.4: Ten days accumulated precipitation (mm, shaded) and corresponding standard deviation anomalies (black contour) of the most anomalous (10 days) case in Portugal – 20 February 1966, corresponding to accumulated precipitation between 11 and 20 February 1966. The standard deviation anomalies were smoothed with the neighbour grid points.

are displayed in Table 2.2. A comparison of the mean magnitudes at different positions in the IP and Portugal revealed that they are greater in the latter, as noted by Ramos (2016).

Ramos (2016) also stated that this phenomenon can be attributed to the larger mean area affected, which is proportionally higher in Portugal than in the IP region. In addition, smaller river basin areas are expected to have higher values of the index due to its basin size dependence (Ramos et al., 2016). This rationale appears justifiable when considering the spatial variability of precipitation in the IP, where precipitation events typically have limited impact on the entire region (Cortesi et al., 2013). One of the most relevant results from Table 2.2 is that, for Portugal, the mean area of the top 100 events above 2 STD is 89% for the 10-day accumulated precipitation period, this result is of the same order

Table 2.2: (a) The mean magnitude and (b) the mean area (A, in percentage) computed for the top 100 events in the Iberian Peninsula and Portugal and for the six rivers basins and for the different accumulated anomalous precipitation rankings.

(a)					
Mean magnitude	1 day	3 days	5 days	7 days	10 days
Iberian Peninsula	94.97	215.77	298.35	363.23	450.59
Portugal	213.99	422.70	584.12	700.73	829.07
Minho	264.70	586.81	802.57	974.56	1131.77
Duero	188.89	378.51	504.60	604.00	707.91
Tagus	186.62	395.47	541.69	639.14	726.65
Guadiana	183.05	355.22	448.39	504.08	555.99
Guadalquivir	183.85	369.56	463.46	531.62	633.42
Ebro	153.99	293.46	359.96	398.93	432.79
(b)					
Mean Area	1 day	3 days	5 days	7 days	10 days
Iberian Peninsula	25.79	42.37	49.23	52.81	58.46
Portugal	58.57	76.97	81.81	85.14	88.75
Minho	74.82	92.64	95.29	96.88	97.44
Duero	54.53	72.81	78.74	82.16	84.14
Tagus	52.57	72.73	76.79	77.49	77.13
Guadiana	47.20	62.39	57.19	54.07	51.28
Guadalquivir	51.39	62.66	60.36	53.70	53.35
Ebro	45.13	61.95	67.49	70.12	72.47

of magnitude as Ramos et al (2016) (93%), indicating that on average, the top 100 events in Portugal affects almost the entire country.

If one focuses the attention to the Portuguese accumulated 10 days ranking, the #1 position (#2 on Ramos et al., 2016) work) belongs to the 20 February 1966 (Figure 2.4). This particular case had an important socioeconomic impact, according to the DISATER database Zêzere et al., 2014, four people died during the 10-day event, while nearly 2000 people were displaced due to floods and landslides. According to Figure 2.4, a 10-day accumulation period resulted in precipitation exceeding 80 mm throughout Portugal. The northern region of the Tagus basin was the most heavily affected, with precipitation values exceeding 360 mm and accumulated anomalies reaching up to 18 STD.

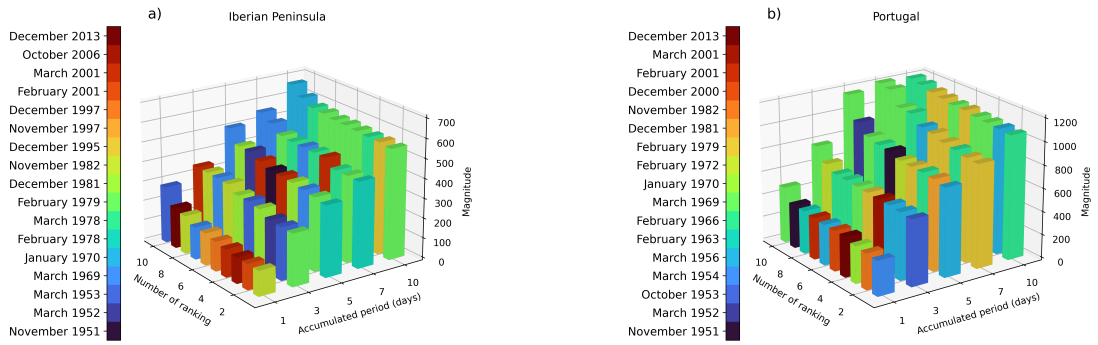

Figure 2.5: The top ten events for each different anomalous accumulated precipitation rankings (1, 3, 5, 7 and 10 days) for the Iberian Peninsula (a) and Portugal (b).

2. RANKING OF MULTI-DAY EXTREME PRECIPITATION EVENTS OVER IBERIA

In the supplementary material it is possible to observed the top nine cases for the IP (Figure A.2), and for Portugal (Figure A.3). Both figures show the percentage of the area above 2 STD dev and their corresponding mean anomalies. These figures serve to confirm the findings reported by Ramos (2016): The February 1979 case had each day mean precipitation anomalies above 2.5 STD dev. It is also important to stress again that the presence of a particular case in the top 10 of the 10-day accumulated precipitation ranking does not necessarily imply an equal representation of any of the individual 10 days in the highest positions for the daily ranking. As an example, in this case, none of the individual days between 11 and 20 February are ranked among the top 10 positions in the daily rank (Figure 2.2). This is one major reason to compute and rank precipitation events considering various multi-day periods and not solely on a daily interpretation. As previously noted by Ramos (2016), it is important to observe that longer temporal scales imply always some "inertia" in the analysis of top-ranks for longer time scales. Therefore, a longer accumulated precipitation period (such as 10 days) would result in several of the top 10 cases being associated with the same precipitation event, although with different cases over a longer period. This is particularly visible in Figure 2.5, where the top ten events for each different anomalous accumulated precipitation rankings over the Iberian Peninsula and Portugal are shown. Regarding IP and Portugal, Ramos et al (2016) identified 16 events that dominate the five top ten events. Here 17 events were identified for both domains, including the December 2013 event that appears firmer on the daily precipitation rank over IP and Portugal (#2 and #7 respectively). It will be shown later that the 24 December 2013 event is related to an AR that crossed over Portugal . It is also important to notice that most of the events (10 out of 17, i.e. 59%; the same order of magnitude presented in Ramos's (2016) work) are coincident for IP and Portugal.

The previous reasoning helps to explain why there are only four distinct events included in the top 10 cases for 10 day period over Portugal, and that took place in 1956, 1966, 1969, and 1979 (Table 2.1b and Figure 2.5b). In fact, these four events dominate the different multi-day rankings, and in particular, the March 1956 event appears in all the different rankings at least once, reaching the highest rank position on a daily and 7-day accumulated period (#5; Figure 2.5b). The February 1966 event, in Portugal, occupies only the #15 position at the daily ranking (#21 in Ramos et al., 2016). However, the 1966 event appeared in the top 10 of the other anomalous accumulated precipitation periods at least twice in each period (Table 2.1b and Figure 2.5b). The March 1969 event is also present in all the different rankings, occupying the #1 position at the daily scale. Finally, the February 1979 event, like February 1966, does not appear on the first ten ranking positions on a daily scale (#43), despite that, appears on the other top ten ranking positions at least once. Overall, results from Table 2.1 and Figure 2.5 reiterate once more the relevance of having a multi-day extreme precipitation events approach.

2.2.1 River Basins

As described earlier, anomalous accumulated precipitation rankings were also obtained for the largest Iberian River basins. Spain and Portugal have constructed several large dams along the main river and tributaries that can control (partially) the river flow. Thus, access to better information on precipitation extremes, including their magnitude, temporal and spatial extent can help the competent authorities to better manage hydrological resources (Ramos et al., 2016). Therefore, the different accumulated rankings have been computed for the six major river basins in the IP (Minho, Duero, Tagus, Guadiana, Guadalquivir, and Ebro), although for the sake of simplicity, only the most relevant results will be presented in this chapter.

Figure 2.6 shows the top event for the ten days accumulated precipitation in each river basin. While in Ramos et al (2016) each river basin presents a different top event, here results obtained for the Tagus and Guadiana basins provide the same top event (#1 event for both basins corresponds to the 11 January 1970). Another notable difference to Ramos et al (2016) work, is that the results comprise more recent extreme precipitation events on Guadalquivir (30 December 2009) and Ebro (26 October 2012), naturally absent in the shorter period analysis by Ramos et al (2016). The most anomalous event (10 days) over

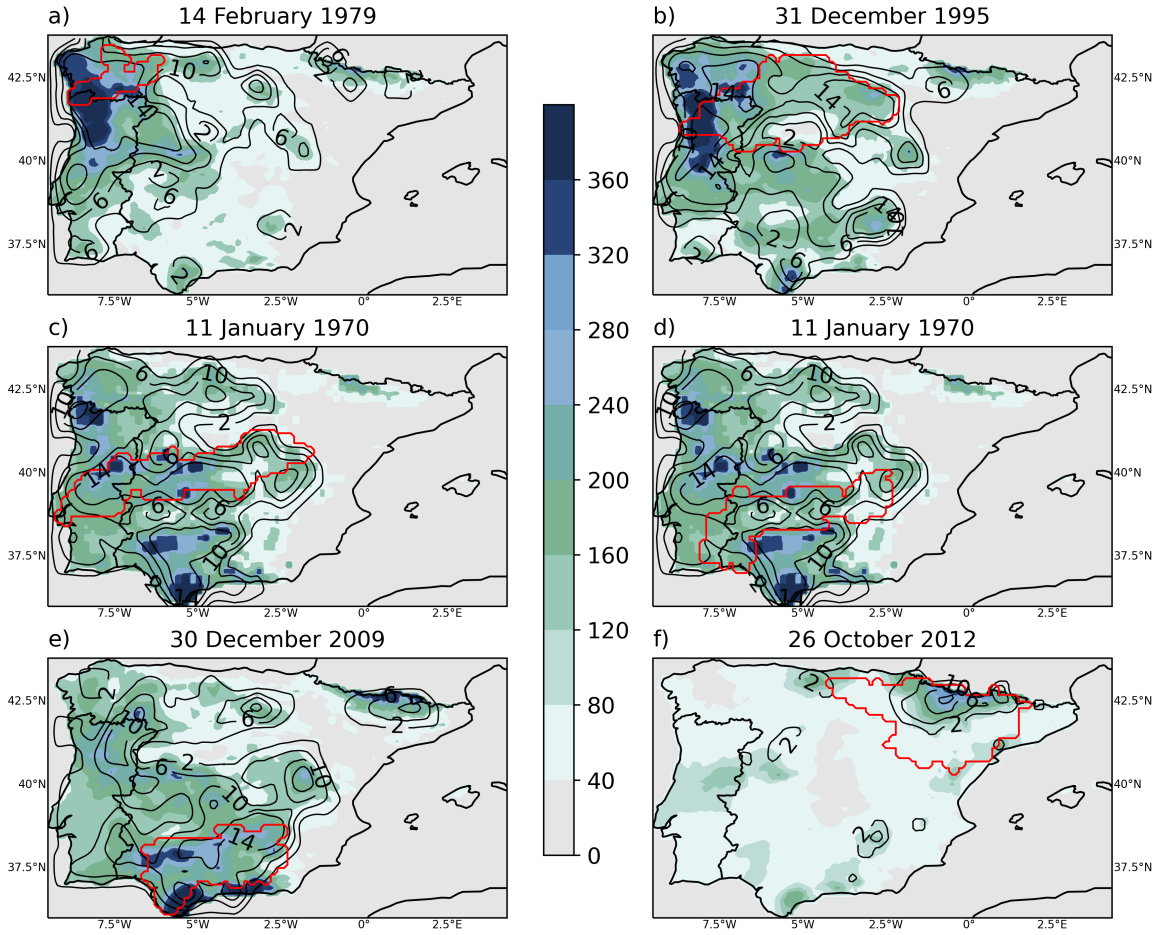

Figure 2.6: Ten days accumulated precipitation (mm, shaded) and corresponding standard deviation anomalies (black contour) of the most anomalous case (10 days) in each river basin. (a) Minho (14 February 1979); (b) Duero (31 December 1995); (c) Tagus (11 January 1970); (d) Guadiana (11 January 1970); (e) Guadalquivir (30 December 2009) and (f) Ebro (26 October 2012). The standard deviation anomalies were smoothed with the neighbour grid points. Each river basin is also highlighted with a thick red contour.

these two basins present in Ramos et al (2016) work occupies different positions in this work (Table A.1: 6 February 1972 #5 and 31 March 1952-#8 events respectively). For the Minho basin, it is possible to observe that the most anomalous case occurred on 14 February 1979, as evidenced in Figure 2.6a. It is notable that a significant portion of the river basin was affected by this event, with 14 STD dev being recorded in most of the region. Moreover, the accumulated precipitation levels exceeded 360 mm over the western part of the basin during this period. In a 10-day accumulated precipitation rank over Portugal, the event that occurred on 14 February 1979 has been identified as the third most significant anomaly (Table 2.1b). For the Minho basin (Figure A.5), six of the ten most anomalous cases correspond to the February 1979 event, and for all the cases on February 1979 event, the mean anomaly recorded over the basin was above 2.5 STD dev. According to Figure 2.6b, the #1 Duero accumulated 10-day case corresponds to 31 December 1995. The spatial pattern of extreme precipitation observed in this case is quite similar to the 14 February 1979 Minho accumulated precipitation pattern. Specifically, in the western part of the Duero basin, where the amount of precipitation reached 360mm, most of the basin experienced 10 standard deviations above the climatology. A deeper analysis of this event shows there was a substantial rise in both the percentage of the area above 2 STD and the corresponding anomaly mean between the 22 and 25 of December 1995 (Figure A.6a; D-9, D-8, D-7, D-6). Despite the similitude of the Minho (Figure 2.6a) and Duero (Figure 2.6b) anomalous accumulated precipitation patterns, their socioeconomic impact was not comparable (Ramos et al., 2016). According to the DISASTER database, the human impacts of the Minho basin #1 were high with a death toll of eight people and hundreds of evacuated people (just in the Portuguese section of the river basin). On the other hand, the Duero basin top event had only a limited socioeconomic impact, not worthwhile to be mentioned. Therefore, it is important to mention that sometimes a precipitation extreme does not need to be necessarily linked to a socioeconomic hazard, it depends on several factors such as the local, soil conditions, and the precipitation distribution along the accumulated period (1, 3, 5, 7 and 10 days). The event that occurred on January 11 1970 is responsible for the #1 position over the Tagus and Guadiana basins, as illustrated in Figure 2.6c, d. Over the Tagus basin, much of the area experienced an anomaly stronger than 10 STD, with the western part reaching as high as 14 STD. In terms of accumulated precipitation, most of the basin recorded values above 160mm, with certain areas reaching above 320mm. As previously mentioned, the #1 Guadalquivir accumulated a 10-day case, which corresponds to December 30, 2009. During this event, the southern part of the Guadalquivir basin experienced accumulated precipitation of up to 360 mm, and there was also widespread intense precipitation observed over the central and western sectors of the Iberian Peninsula (Figure 2.6e). For the Ebro basin, the most extreme case (26 October 2012) does not reach high levels of precipitation compared to the other hydrographic basins. However, it should be noted that accumulated precipitation values of around 200 mm correspond to up to 10 STD anomalies in the Pyrenees sector. When the top ten events for each different anomalous accumulated precipitation ranking were examined for each river basin (Figure 2.7), the first noticeable conclusion was that the same precipitation events occupied several positions, sometimes in a more consistent way than what was found for the larger IP and Portugal domains (Figure 2.5). The Minho, Tagus, and Guadalquivir basins show a similar pattern. Some noteworthy examples include the Minho basin, where six of the top 10 cases in the 10-day ranking correspond to the same period (February 1979), even though this event is not among the top ten for other accumulated rankings, as in Ramos et al (2016) study. This result, once more, reinforces the importance of employing multi-day ranking analysis. The results show that for the Tagus and Ebro basins, the uppermost positions in the rankings are predominantly attributed to two anomalous periods - specifically, February 1972 and March 1974 for the Tagus and Ebro basins, respectively. However, for the Ebro basin, while in Ramos et al (2016) work, the first seven top positions

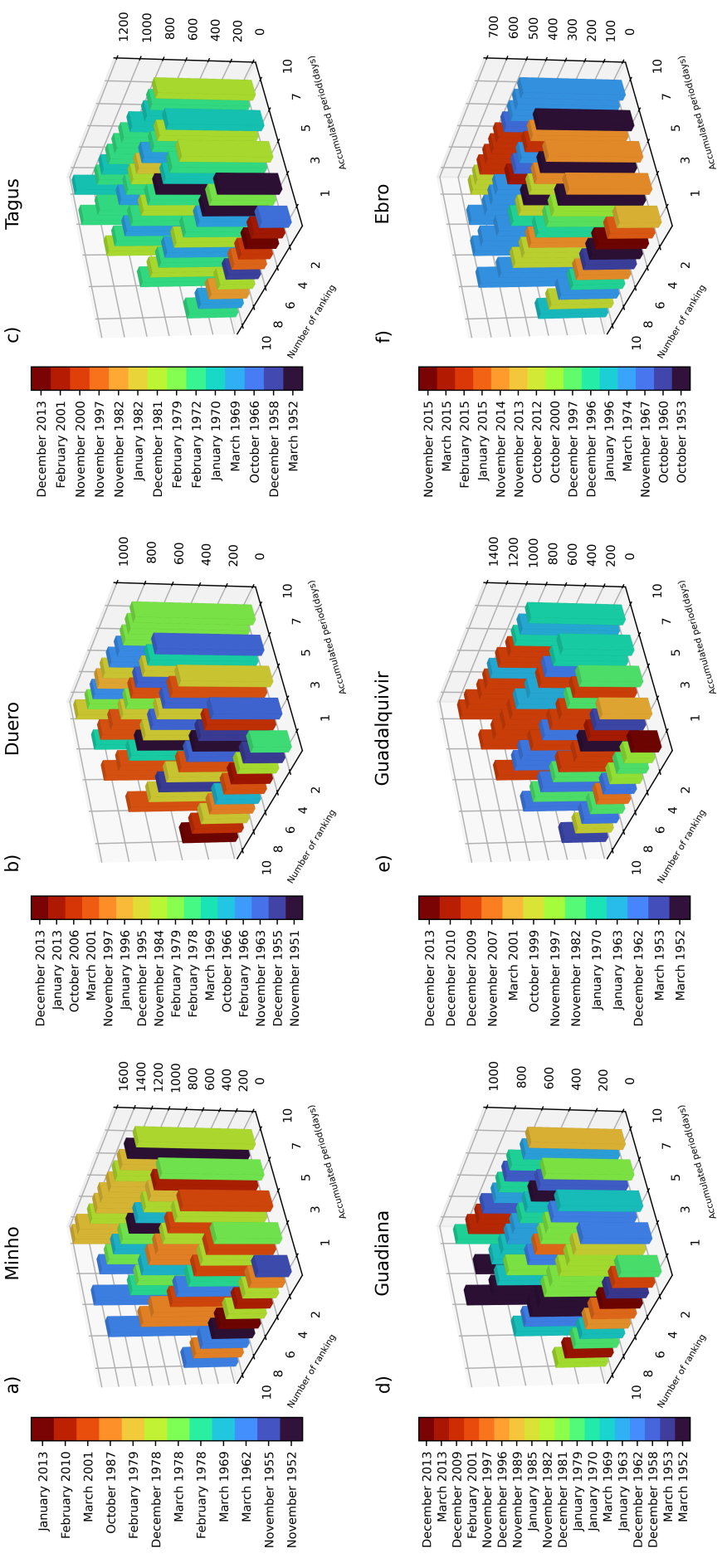

Figure 2.7: The top ten events for each different anomalous accumulated precipitation rankings (1, 3, 5, 7 and 10 days) for each river basin: Minho (a), Duero (b), Tagus (c), Guadiana (d), Guadalquivir (e) and Ebro (f).

for the 10-day accumulated period were occupied by the March 1974 event, results obtained here show that these positions have been replaced by more recent events. In particular, October 2012 occupies the first two positions, and the February 2015 event occupies the remaining five positions (Table A.1). The presence of more recent events (after 2008) in the multi-day ranking for overall river basins, constitutes a significant difference from the findings reported by Ramos et al (2016). In the rankings of the 5, 7, and 10 days accumulated period over the Guadalquivir basin, in Ramos et al (2016) work, the top positions of these accumulated periods were occupied by December 1962 and January 1963. Although these events are also included in this revised assessment, the majority of the top positions over 5,7, and 10 days accumulated period are occupied by the December 2009 event. Of the first seven positions for the 10-day accumulated period, only the sixth (in January 1963), does not belong to the December 2009 event (Table A.1). A closer analysis of Figure A.8 shows that this event is mainly dominated by 21, 23, and 25 of December anomalous precipitation. Based on further analysis, it has been determined that the extreme precipitation event that occurred in December 2009 over the Guadalquivir basin is linked to the passage of two ARs in the southern region of the Iberian Peninsula. Detailed information regarding this relationship will be presented in the following sections.

2.3 Summary

The main conclusions from this chapter can be summarized as follows:

- The methodology developed for computing daily to 10-day rankings has proven to be valuable for studying multi-day accumulated precipitation rankings across the eight different domains considered.
- The diverse rankings databases obtained for different domains and time scales are useful for various studies aimed at understanding the causes and impacts of extreme precipitation periods covering relatively large areas. This utility extends to hydrologists, water resources managers, and insurers of socioeconomic activities, such as agriculture or hydroelectricity production from renewable sources (currently responsible for up to 30% of total electricity production in Portugal).
- Across different domains, it was observed that a few events typically dominate the top ten rankings. This dominance by a limited number of extreme precipitation episodes at longer time scales is primarily a result of analyzing successive accumulated precipitation days over extended periods.
- Examination of rankings relative to six different river basins revealed that the top ten precipitation episodes are largely non-coincident, emphasizing the spatial variability of extreme precipitation phenomena in the study area (Ramos et al., 2016).
- The methodology employed in constructing the rankings allows for the identification of extreme cases based on particularly high precipitation totals, extensive areas affected by less extreme precipitation values, and persistent rainy conditions over longer periods. This diversity enables a nuanced analysis of extreme precipitation events.

Chapter 3

Atmospheric rivers detection and analysis

3.1 Datasets and Methodology

3.1.1 ERA-5 Reanalyses dataset

As stated previously, the second major objective of this work is focused on the use of an automated detection algorithm to detect atmospheric rivers (ARs) in the North Atlantic Ocean basin using state-of-the-art ERA-5 reanalysis. This detection tool will enabled to identify and conduct a comprehensive analysis of major AR events that impacted the Iberian Peninsula (IP) from 1959-2022. Understanding the atmospheric water cycle complexity is crucial in meteorology and hydrology (Gimeno et al., 2012). Moisture transport, particularly through ARs, plays a key role in extreme precipitation events in Western Europe (Lavers and Villarini, 2013, Ramos et al., 2015). The algorithm by Ramos et al (2015), initially developed with ERA-interim reanalysis, has been adapted to the higher resolution ERA-5 dataset for improved accuracy. In particular, utilizing the zonal and meridional components of the vertically integrated horizontal water vapour transport (IVT) flux and mean sea level pressure during the extended winter months of ONDJFM. To capture the longest possible climatological period, data from the 1959-2022 time-frame was obtained, with a temporal resolution of 6 hours and a spatial resolution of 0.25º latitude-longitude grid.

3.1.1.1 ARs identification

The majority of the studies identify using the IVT variable (Ramos et al., 2015). As mentioned before, the ERA-5 dataset was used which already included the zonal and meridional components of the vertically integrated horizontal water vapour transport for the entire column of the Atmosphere computed from the surface to the top in an Eulerian framework (e.g., Neiman et al., 2008; Lavers et al., 2012):

$$\mathrm{IVT} = \sqrt{\left(\frac{1}{g}\int_{\mathrm{surf}}^{\mathrm{top}} qu\,dp\right)^2 + \left(\frac{1}{g}\int_{\mathrm{surf}}^{\mathrm{top}} qv\,dp\right)^2} \tag{3.1}$$

where q is the layer-averaged specific humidity ($\mathrm{kg},\mathrm{kg}^{-1}$); u and v are the layer-averaged zonal and meridional winds (ms^{-1}), respectively; g is the acceleration due to gravity; and dp is the pressure difference between two adjacent pressure levels.
Similar to the approach employed by Ramos et al (2015), the identification of ARs that may affect the IP (35º– 45ºN, 10ºW) was done based on the following set of criteria:

- The maximum IVT at 12:00 UTC for each day within the IVT dataset (1959-2022) was deter-

mined along the 10ºW meridian and between 35º- 45º N to compute the IVT threshold. According to previous authors, the 85th percentile is appropriate to detect the most intense IVT values in Europe(Ramos et al., 2015; Lavers and Villarini, 2013; Lavers et al., 2012). The 85th percentile of the maximum IVT distribution (506 $\mathrm{kg\,m^{-1}\,s^{-1}}$) was computed and used as the threshold value for the first step in the identification of ARs.

- At each time step (every 6 hours) in the IVT dataset (1959-2022), the maximum IVT value and their location on grid points between 35º and 45ºN along 10ºW are extracted.
- If the maximum IVT from phase 2 exceeded the 85th percentile (>506 $\mathrm{kg\,m^{-1}\,s^{-1}}$), that particular grid cell was identified as a potential AR. Then, a Westward/Eastward search to identify the maximum IVT at each longitude and tracked the location for the grid points where the IVT threshold (as derived for 10ºW) was exceeded. The maximum IVT value at each grid point was compared to the IVT 85th percentile obtained in the first step. If the maximum IVT value exceeded the IVT 85th percentile, the corresponding grid point was added to the AR central core. The core must extend over many degrees of longitude in order to obtain results consistent with studies carried out by other authors such as Ramos (2015). Thus, using ERA-5 data, the length should correspond approximately to 80 continuous longitude pixels (80*0.25º = 20º 1700 km) with IVT values above 506 $\mathrm{kg\,m^{-1}\,s^{-1}}$. The AR central core for a particular time-step having been identified, the algorithm then verified in subsequent time-steps if it continued to fulfil the conditions outlined in phases 2 and 3.

By applying these three methodological steps, numerous potential ARs close to Iberia can be detected. However, for the remaining of this analysis, only persistent events are considered, and therefore an additional temporal criteria must be considered. According to Ramos et al (2015), for a persistent AR event to be identified, it needs to meet the following requirements: 1) it must be detected for at least 18 hours (3 timesteps in the dataset), and 2) if there is a gap of more than 1 day, it indicates the occurrence of two independent AR events.

3.1.1.2 Large-scale atmospheric circulation pattern indices

In the subsequent phase of the study, following the identification and analysis of all detected ARs and their characteristics, attention was turned to the circulation patterns associated with these events. To that end, monthly mean indices from the Climate Prediction Center (CPC) of the National Oceanic and Atmospheric Administration (NOAA) for the years 1959-2022 were employed. These indices were computed from the 500 hPa geopotential height field for the entire Northern Hemisphere ($20^\circ - 90^\circ$N) using rotated principal component analysis (PCA; Barnston and Livezey, 1987), and include the North Atlantic Oscillation (NAO), East Atlantic (EA), East Atlantic/Western Russia (EA/WR), Scandinavia (SCAND), and Polar/Eurasia (POL), as previously used by Ramos et al (2015). The extended winter mean indices for each year were considered in the same way as in the aforementioned study. For a given year N, the monthly means of October-December (OND) corresponding to year N-1 and January-March (JFM) of the year N were considered. For instance, for the extended winter of 2021, compromises the monthly means of OND 2020 and JFM 2021 .

3.1.2 AR climatology

After applying the methodology as described above, a climatological assessment of ARs was undertaken using only the persistent AR events (i.e., restricting the ARs to those that have at least 18 hours

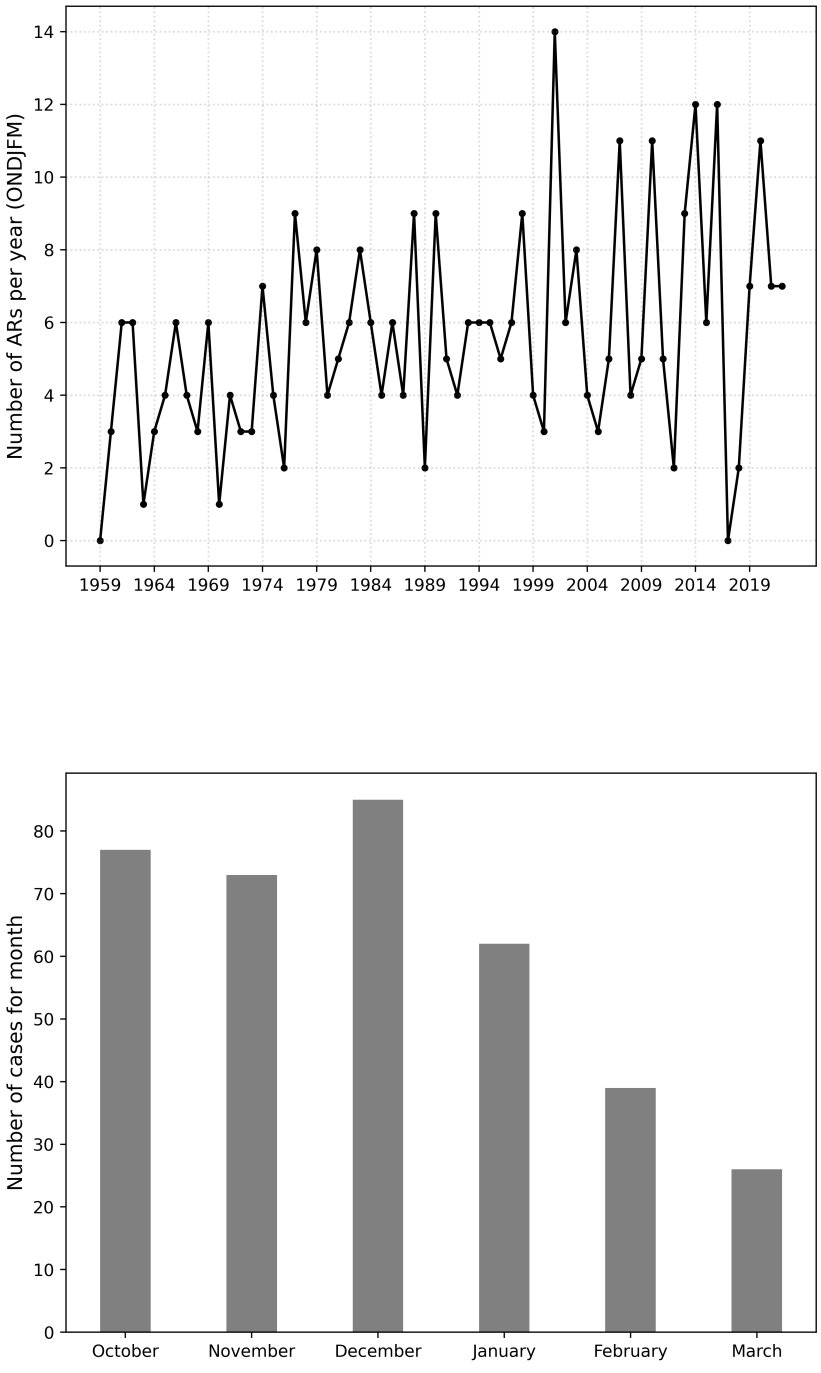

Figure 3.1: (a) Interannual variability of the number of ARs per extended winter (ONDJFM) and (b) intra-annual variability of the number of ARs from 1959 to 2022 over the IP.

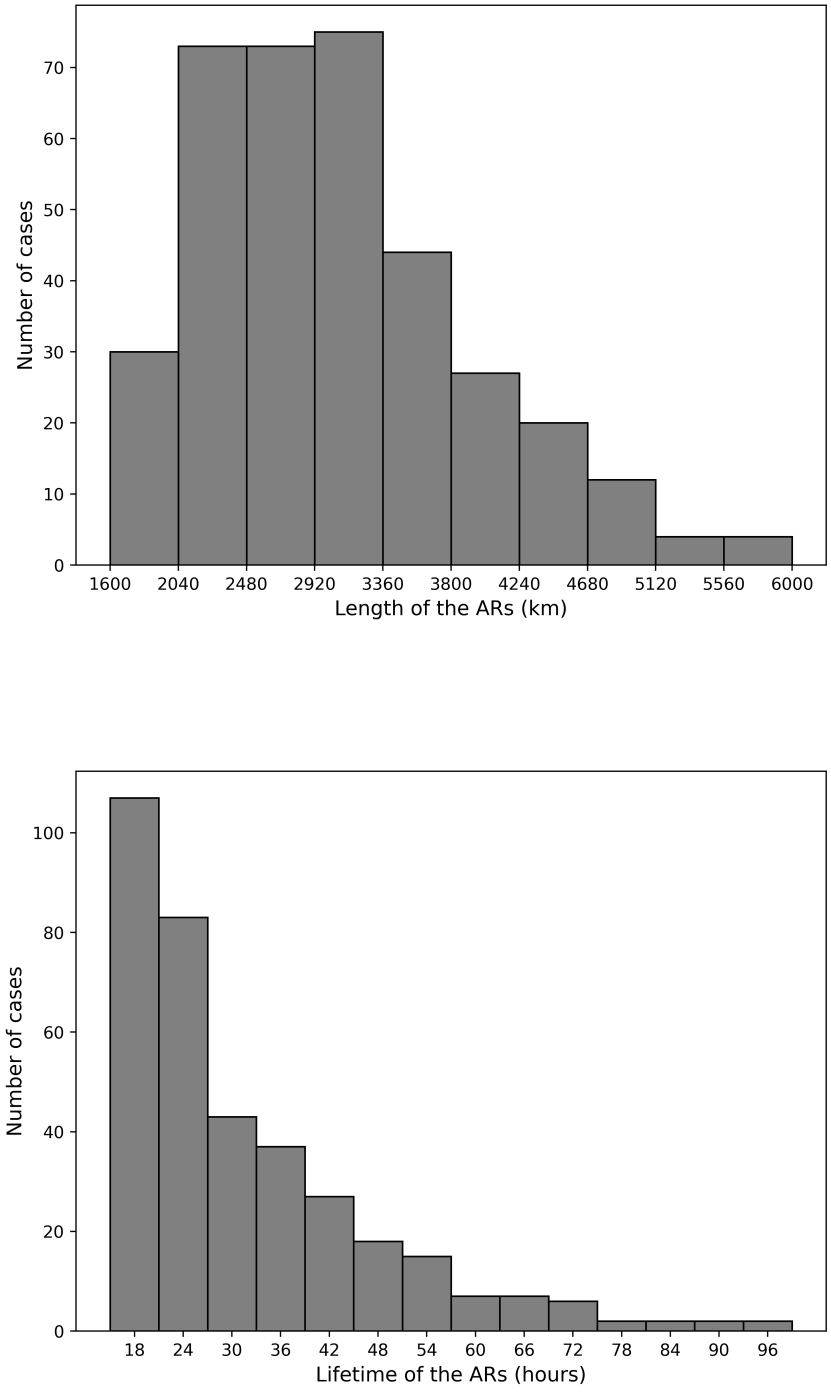

Figure 3.2: Distribution of the (a) length of the ARs (Km) and (b) number of time steps (h) per each persistent AR.

of persistence) that make landfall over the IP. In the analysis, a total of 363 persistent AR events were recorded, corresponding to an annual mean value of ~ 5.7 yr^{-1}(~ 8.2 yr^{-1} on Ramos et al (2015) using ERA-Interim from 1979 to 2012). The interannual variability is present in Figure 3.1a, where it is noteworthy that in the analysis, the extended winter mean year N was computed considering the monthly means of the OND from year N - 1 and JFM from year N. Despite a considerable amount of variability observed over the years, it is crucial to emphasize that the highest number of AR occurrences was recorded during the extended winter of 2001, with 14 ARs identified. Furthermore, during the extended winters of 1959 and 2017, no ARs were detected. It is worth noting that for the year 1959, data were only available for the last months of 1958 and only available for the months of January, February, and March of 1959. In addition, certain extended winters are noteworthy, such as 2010, which recorded 11 ARs and was marked by intense precipitation in the Iberian Upon qualitatively examining the time series, it is apparent that there is a positive trend in the number of identified ARs over the years, particularly when excluding the extended winter of 2017, which represents the minimum number of occurrences in the dataset. The analysis of intra-annual variability for the 1959-2022 period was also conducted (Figure 3.1b). Based on the figure, a similar conclusion can be drawn as in Ramos et al (2015), which is that the number of ARs per month begins to decrease between December and March, having peaked in December with 85 ARs detected. Ramos et al (2015) propose that the reduction in the number of ARs towards the end of winter could be associated with the weakening and a shift to the north of the storm track in the North Atlantic as spring sets, resulting in a decrease in moisture transport Trigo, 2005. Additional features were computed to characterize the ARs that make landfall over the IP, such as length, duration, and location distributions. Based on the analysis of Figure 3.2a, it can be concluded that the most frequent AR lengths observed falls between 2040 and 3360 km. Furthermore, the number of AR events drastically reduces as the length of an event increases beyond this range. These long structures are in line with the current understanding of the AR that can extend for thousands of kilometres and, sometimes, even across the entire ocean basin (Ralph and Dettinger, 2011). Upon analysing the duration of the detected AR events (as shown in Figure 3.2b), it is noteworthy that the number of time steps also decreases rapidly. Specifically, it was observed that out of the 363 ARs detected, 190 of them (approximately 52.5% of the total), have a duration of less than 24 hours (i.e., 4 consecutive time steps). In accordance with the previous statement, the total number of persistent ARs identified during the 1959-2022 period was 363, which, accounting for the duration of each AR and the 6-hour time steps, corresponds to 2357 time steps. Figure 3.3 displays the distribution of the maximum IVT location, ranging from 35º to 45ºN and along the N-S longitude line of 10ºW, for all of the AR time steps. The figure suggests that the AR core is mainly situated at higher latitudes during persistent AR events. However, a more complete understanding will be gained by analysing Figure 3.4. In the final step of the analysis, the averages for the sea level pressure (SLP) and IVT intensities were computed using every time step that corresponds to an AR event that affects the IP and compared with the extended winter long-term mean (Figure 3.4). Figure 3.4a shows the average pattern for the extended winter months, revealing the expected low-pressure system near Iceland (below 1002 hPa) and the Azores anticyclone high pressure above (1020 hPa), which is located between the Azores archipelago and IP. Analysing the IVT mean pattern for the extended winter months, values between 200 and 325 kg m^{-1} s^{-1} were observed on a large band crossing the entire North Atlantic Ocean basin (67º- 25ºN, 80º- 10ºW), being advected from west-southwest to east-northeast. When considering the associated pattern during the occurrence of the persistent ARs (Figure 3.4b), it is apparent that the low-pressure center identified in Figure 3.4a intensifies further, reaching 990 hPa, and shifts towards a position closer to the United Kingdom. This movement is associated with ARs connected to extra-tropical cyclones. In turn, the Azores anticyclone

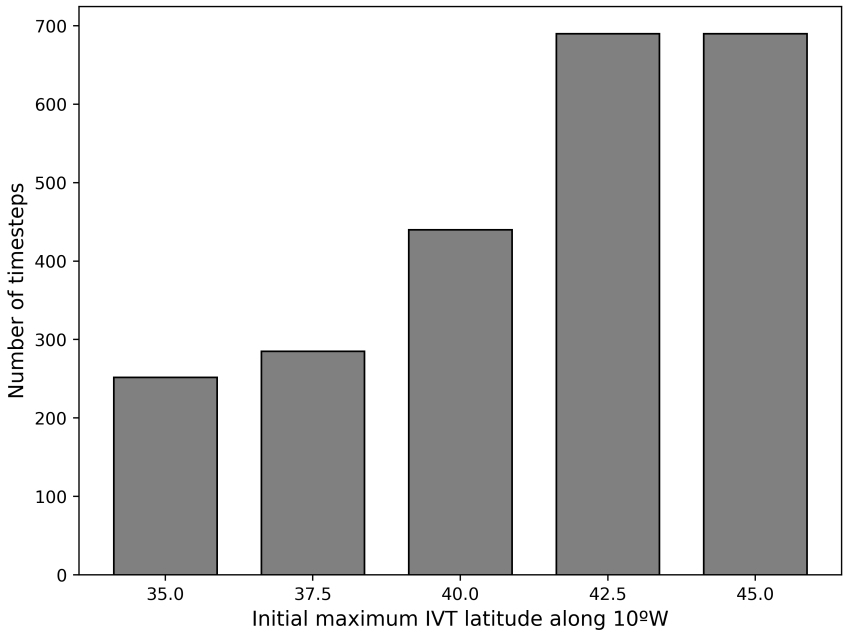

Figure 3.3: Distribution of the location of the max IVT between 35° and 45° N and along 10°W for all the ARs timesetps

appears stronger in the southwest part of the IP. Perhaps the difference that is immediately apparent is the magnitude of the IVT values. Globally, the branch over the entire North Atlantic Ocean is more intense in comparison with Figure 3.4a, especially near the northwest coast of the IP, reaching values of 500 $\mathrm{kg\,m^{-1}\,s^{-1}}$ and advection terms from west-southwest to east-northeast also gain more expression.The anomalies between the extended winter (ONDJFM) long term-mean and the composite for the AR time steps were also computed (Figure 3.4c). The results of this analysis reveal the presence of negative SLP anomalies centered over Ireland and reaching values as low as -18 hPa. Additionally, it is noted a positive anomalous SLP pattern over northern Africa. With regards to IVT anomalies, it is possible to observe two major branches with different signs. The dipole pattern can be observed with negative values located west of the British Isles, and positive values covering a lower section of the North Atlantic Ocean with a northeast orientation, and attaining greater magnitudes over the northwestern coast of IP. Furthermore, it is noteworthy to emphasize that the positive anomalies reach higher values (350 $\mathrm{kg\,m^{-1}\,s^{-1}}$) than their negative counterparts (-100 $\mathrm{kg\,m^{-1}\,s^{-1}}$), indicative of the presence of an asymmetric dipole structure. Overall, this configuration is in line with the results obtained by other authors such as Ramos et al (2015) and Lavers and Villarini (2013).

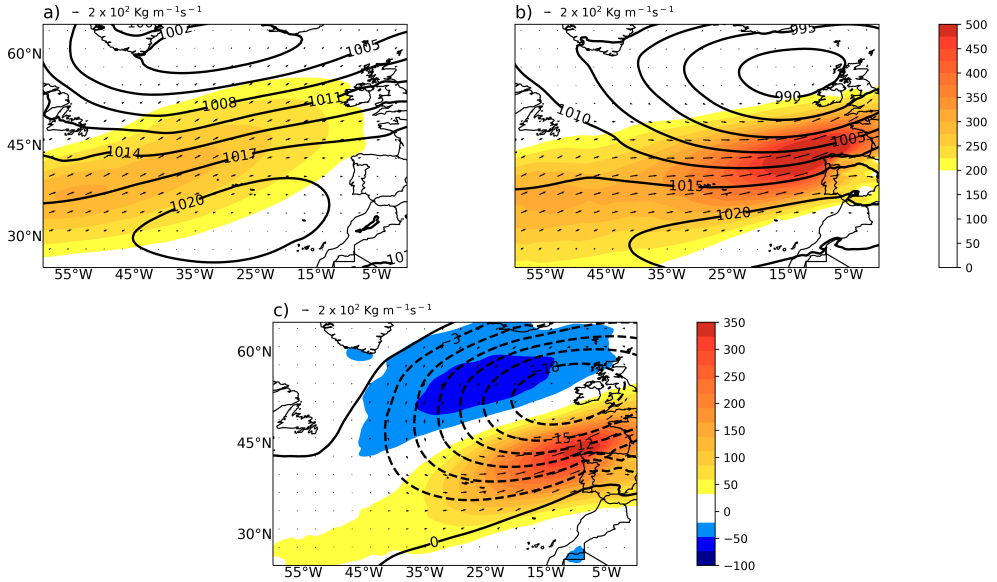

Figure 3.4: (a) Extended winter (ONDJFM) long-term mean (1959–2022) of the IVT direction (vectors) and intensity ($\mathrm{kg\,m^{-1}\,s^{-1}}$; color shading) and SLP (hPa; contours) fields; (b) Mean composites of IVT direction (vectors) and intensity ($\mathrm{kg\,m^{-1}\,s^{-1}}$; color shading) and SLP (hPa; contours) fields during the occurrence of the persistent ARs that affect the IP (363 persistent cases corresponding to 2357-time steps); (c) The anomalies between the long-term mean and the AR composites.

3.1.3 Relationship between Iberian ARs and large-scale atmospheric circulation patterns

This section aims to quantify the relationship between large-scale atmospheric circulation patterns and the occurrence of ARs, based on the approach employed by Ramos et al (2015). Thus, correlation coefficients were computed between the number of persistent ARs per extended winter season (ONDJFM) and the circulation indices that describe the temporal variability of the main atmospheric circulation pattern affecting Europe (NAO, EA, EA/WR, SCAND, and POL) for the period of 1959-2022. The results of this analysis are presented in Table 3.1, indicating that statistically significant correlations at the 5% significance level were only observed for the Eastern Atlantic (EA) pattern, which displays a positive correlation. Specifically, a statistically significant positive correlation (0.437) at the 5% significance level was observed only for the EA pattern, while the Polar/Eurasia pattern had a non-significant negative correlation (-0.205) with a p-value of 0.148. It is noteworthy that the correlation values for the two patterns obtained in the current study at the 5% significance level are comparable to those obtained by Ramos et al (2015) although that study considered the period spanning the years 1950 to 2011. In summary, the approach taken to assess the relationship between atmospheric circulation patterns and AR occurrence involved computing correlation coefficients between the number of persistent ARs and various atmospheric circulation pattern indices. The results indicate that a statistically significant positive correlation was observed only for the Eastern Atlantic (EA) pattern. The findings differ somewhat from those reported in a previous study by Ramos et al (2015), although the correlations obtained at the 5% significance level were similar.

Table 3.1: Correlation analysis during the 1959–2022 extended winter months between the number of ARs and the large-scale atmospheric circulation pattern. Statistically significant correlations are highlighted in boldface.

	NAO	EA	EA/WR	SCAND	POL
Correlation	-0.049	0.437	0.076	0.150	-0.205
p value	0.730	0.001	0.595	0.287	0.148

3.2 Summary

The key findings from this chapter can be succinctly summarized as follows:

- An automated detection algorithm for identifying ARs in the North Atlantic Ocean basin using ERA-5 reanalysis was developed.
- In the analysis, a total of 363 persistent AR events were recorded, corresponding to an annual mean value of $\sim$6 ARs per year. It was observed that out of the 363 detected ARs, approximately 52.5% (190 events) have a duration of less than 24 hours (i.e., 4 consecutive time steps). The observed lengths of ARs fall primarily within the range of 2040 to 3360 km. Additionally, the number of AR events significantly decreases as the duration and length of an event increases beyond this range (24 hours and 3360 km).
- During persistent AR occurrences, a composite analysis reveals negative SLP anomalies centered in Ireland and positive anomalies over northern Africa. This robust SLP gradient configuration is crucial for the rapid moisture advection toward the IP associated with ARs. This configuration aligns with the outcomes observed by Ramos et al (2015). The ARs impacting the IP are notably linked with the EA pattern, with a weaker influence from patterns such as the North Atlantic Oscillation (NAO) or Scandinavian (SCAND).

Chapter 4

Iberian extreme precipitation and Atmospheric Rivers

4.1 Categorize Atmospheric Rivers

Max IVT (kg m^{-1} s^{-1})	Duration of an AR conditions (h)		
	≤ 24	$\geq 24-48$	≥ 48
≤ 250	Not an AR	Not an AR	Not an AR
$\geq 250-500$	Weak AR	Cat 1	Cat 2
$\geq 500-750$	Cat 1	Cat 2	Cat 3
$\geq 750-1000$	Cat 2	Cat 3	Cat 4
$\geq 1000-1250$	Cat 3	Cat 4	Cat 5
≥ 1250	Cat 4	Cat 5	Cat 5

AR Category scale
Cat 1: Primarily beneficial
Cat 2: Mostly beneficial, but also hazardous
Cat 3: Balance of beneficial and hazardous
Cat 4: Mostly hazardous, but also beneficial
Cat 5: Primarily hazardous

Table 4.1: (top) An AR intensity scale based on maximum instantaneous IVT magnitude and duration of AR conditions, and (bottom) a subjective assessment of the potential for beneficial or hazardous impacts Ralph (2019)(2018).

The ranking of multi-day extreme precipitation events over the Iberian Peninsula (IP), covering the period from 1950-2015, was presented in section 2 using a similar approach as Ramos et al (2014; 2016). Subsequently, an automatic algorithm was applied to identify Atmospheric Rivers (ARs) in section 3, making good use of the high temporal and spatial resolution of ERA-5 reanalysis data for the period spanning 1959-2022. This section involves quantifying and determining to what extend large rainfall amounts are well associated to the passage of ARs in the North Atlantic region during the period of 1959-2015, which is commonly available to both datasets.

The initial step of the analysis involved the categorization of ARs into various groups. This classification was based on previous research (Ralph et al., 2019; Ralph and Dettinger, 2011; Eiras-Barca et al., 2021). Ralph et al (2019) proposed a strategy for scaling ARs by considering the roles of Integrated Vapor Transport (IVT) maximum magnitude and the duration of AR conditions in generating high-impact hydrometeorological events. According to these authors, AR events are categorized based on the maximum instantaneous IVT intensity and the duration of the event at a given point across the considered coastal

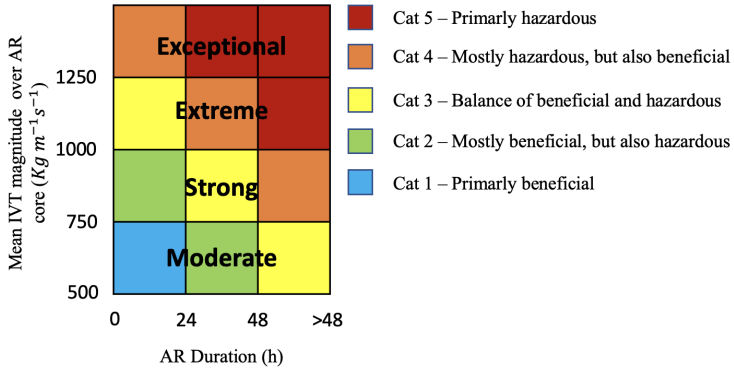

Figure 4.1: Scale that categorizes AR events based on the mean IVT magnitude over AR core during the event associated with the duration of the AR event (Adapted from Ralph et al (2019) work).

grid cells (Ralph et al., 2019), as shown in Table 4.1.

An AR event at a given location is categorized by locating the row associated with the maximum IVT and the column associated with the event duration. For example, a maximum IVT $\geq$500 and $<$750 $\mathrm{kg\,m^{-1}\,s^{-1}}$ would be classified as being of "moderate" intensity, and an intermediate duration $\geq$24 and $<$48 h would rank this as an AR cat 2 event. The concept of categorizing ARs was adopted following the approach presented in Table 4.1 by Ralph et al (2017). However, while Ralph et al (2017) established his classification considering only the coastal grid cells affected, here an important change was adopted. Instead of categorizing AR events only based on the maximum instantaneous IVT intensity at a specific time step, this study uses the mean IVT value along the entire core of the AR during the persistent event for categorization. The same temporal factor as Ralph et al (2017) will be used for the second term of the categorization, which is the AR duration (in hours). Therefore, as shown in Figure 4.1, the two main assumptions (intensity and duration of all ARs) remain the same and are visible in the coloured AR scale (Figure 4.1). However it is important to take in attention that on the AR scale, the maximum Cat is AR Cat 5, even if the event duration is equal to or greater than 48 hours. It is crucial to emphasize again that the initial criterion for the automated detection of ARs entails that a grid cell must surpass the 85$^{\mathrm{th}}$ percentile threshold (506 $\mathrm{kg\,m^{-1}\,s^{-1}}$, as outlined in section 3.1.2) to be considered part of the AR core. It much be stressed that events longer than 24 h and with mean IVT core lower than the 85$^{\mathrm{th}}$ percentile. Four examples of the results obtained from the direct application of the AR Category scale are presented in Figure 4.2a, b for two specific timesteps (1988-02-05 06:00 UTC, 1996-01-06 06:00 UTC) during two AR persistent events classified as Cat 1. Additionally, Figure 4.2c, d displays timesteps during ARs events classified as Cat 5 (1985-11-05 18:00 UTC, 2013-12-24 00:00 UTC, respectively). The difference in the patterns associated with Cat 1 and Cat 5 becomes apparent in Figure 4.2. In these examples, it is observed that the IVT intensity values over the AR core reach magnitudes in the range of 600-700 ($\mathrm{kg\,m^{-1}\,s^{-1}}$) for Cat 1 events (Figure 4.2a, b), while for Cat 5 events (Figure 4.2c, d), the IVT magnitude values practically double to 1200-1400 ($\mathrm{kg\,m^{-1}\,s^{-1}}$). Overall, the IVT direction (vectors) is dominated by flows from the west that get more intense over the AR core and naturally reaches stronger magnitudes in Cat 5 cases. However, two independent AR structures can be identified in the 1988 (Cat 1) and 1985 event (Cat 5), although the automated AR detection algorithm only identified the eastern structure Figure 4.2b, c). This is because the focus of the study is on ARs that make landfall over the IP. Therefore, the automated detection algorithm used does not consider western structures. However, one must acknowledge that the western structures of ARs are also deemed significant, as they can potentially result

in extreme precipitation events along the North American east coast or travel across the Atlantic Ocean and impact the West coast of the European continent. Conversely, the 2013 event presents a perfect example of an AR event that starts over the North American eastern coast, that than passes through the entire Atlantic, reaching the sector north of Europe and that it's a clear case where ARs were responsible for a huge amount of the meridional WV transport in the midlatitudes(Ramos et al., 2015; Peixoto and Oort, 1992; Zhu and Newell, 1998).

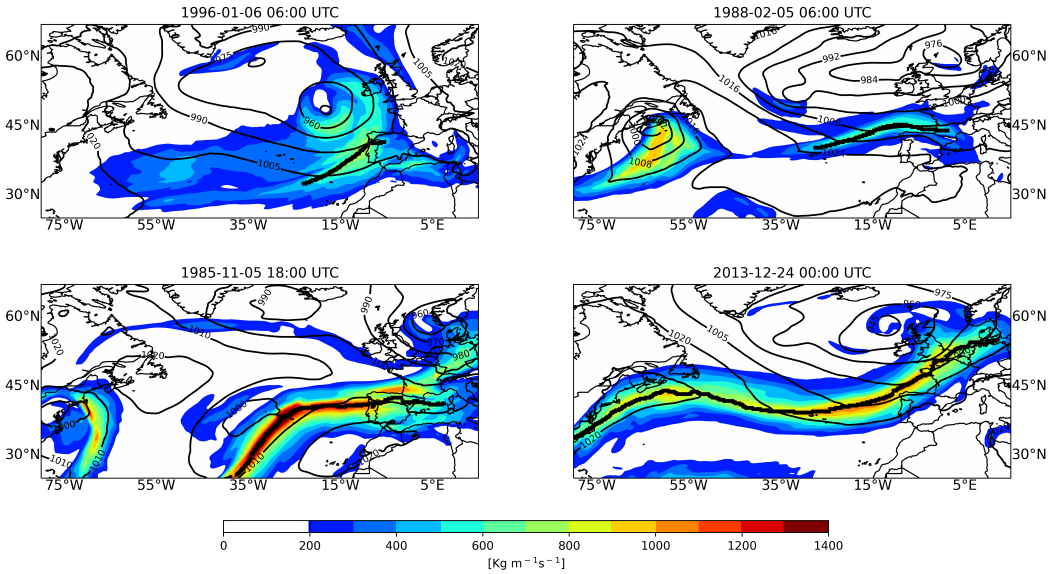

Figure 4.2: Integrated Water Vapor Transport (IVT) intensity ($\mathrm{kg\,m^{-1}\,s^{-1}}$; color shading) and SLP (hPA, contours) fields, and Atmospheric River core detected by the Algorithm (scatters) of a timestep during an AR event categorized as Cat 1 (a, b; 1996-01-06 06:00 UTC, 1988-02-05 06:00 UTC) and Cat 5 (c, d; 1985-11-05 18:00 UTC, 2013-12-24 00:00 UTC).

4.1.1 Decadal Analysis of Atmospheric Rivers by Intensity Category

Table 4.2 provides a comprehensive overview of the number of ARs per decade, categorized by their intensity level or Category. Each row represents a different category (Cat 1 to Cat 5), while the columns denote specific decades from 1960 to the year 2022. The numerical values in the cells represent the count of ARs falling within each category during the respective decades.

Observing the data, we can discern trends in AR occurrence over the decades. For instance, it appears that Cat 2 ARs exhibit a notable increase in frequency over time, peaking in the 2000-2009 decade. In contrast, Cat 1 ARs show a relatively consistent occurrence across the years, with a slight decrease in the more recent decades. Categories 3 and 4, on the other hand, display variable patterns, with some decades witnessing higher counts than others.

The 'Total' row at the bottom provides an aggregate count of ARs across all categories for each decade. It is evident that there has been a general increase in the total number of ARs over the years, reaching its highest point in the 2010-2019 decade.

This detailed breakdown allows for a nuanced understanding of the historical distribution of ARs, shedding light on both long-term trends and potential fluctuations in their occurrence across different intensity categories.

Table 4.2: Number of ARs per decade grouped by Category since 1960

Period	1960-1969	1970-1979	1980-1989	1990-1999	2000-2009	2010-2019	2020-2022
Cat 1	7	10	9	12	7	4	2
Cat 2	9	18	13	20	25	24	6
Cat 3	15	11	16	12	12	21	7
Cat 4	9	6	8	9	16	12	7
Cat 5	2	2	8	7	3	5	3
Total	42	47	54	60	63	66	25

4.2 Quantify the relation between AR events and multi-day precipitation extreme events.

Once a category scale for ARs is established, it is possible, together with the information about the Ranking of multi-day extreme precipitation events to search for a meaningful assessment on the links between these independent datasets. The theoretical reasoning behind this relationship suggests that a stronger AR (as measures in the AR category scale) will often imply stronger precipitation upon landfall. However, in some cases, a stronger AR does not necessarily result in stronger precipitation values. The reason for this can be as simple as the AR not crossing over a critical area, that it had a short pass, or the thermodynamic conditions are not favourable for the occurrence of precipitation. For simplicity, we will only present the analysis to the entire IP and Portugal, although it is worth noting that each river basin (Minho, Duero, Tagus, Guadiana, Guadalquivir, Ebro) can also be assessed individually.

In the first approach, a search was conducted over a list of ARs to identify any correlation with the ranking of multi-day extreme precipitation events (identified in section 2). Upon conducting a more detailed analysis, it was found that it would be better to consider only those AR events that not only matched with an accumulated precipitation event but also had their passage confined to latitudes below 43ºN (thus making landfall clearly over the IP). Figure 4.3a provides the magnitude of the 10-day accumulated precipitation extreme distribution for each category of AR defined previously in a violin plot representation. A violin plot is a type of data visualization that combines the features of a box plot and a kernel density plot. It is used to display the distribution of data and provide information on its probability density (Moon, 2016). The most general conclusion drawn from this figure is that, under favourable conditions, an AR will often correspond to a precipitation extreme. This visual aid also enables us to confirm that, in general, an increase in the intensity of an AR corresponds with a corresponding increase in the magnitude of the associated precipitation extreme (Figure 4.3a). It is important to notice that only ARs that match with an entrance in the precipitation extreme ranks are considered for these results. Therefore the number of impacting ARs per category is not constant, as shown in Figure 4.3b.

From Figure 4.3b, it can be inferred that the most statistically significant results are linked to ARs that are classified as Cat 2, Cat 3, and Cat 4. Therefore, it is important to recognize that these categories of AR have a higher likelihood of contributing to a precipitation extreme event than other categories. Overall, one can state that an increase in the maximum values of precipitation magnitude is observed for stronger AR classes. As an illustration, for ARs categorized as Cat 1, the maximum precipitation extreme for a 10-day accumulation period has a magnitude of 321.54, and corresponds to the #160 position (January 6 1996). On the contrary, the most extreme accumulated precipitation in this study is linked to an AR that began on February 4 1979 at 00:00 UTC, and ended on February 10 at 12:00 UTC (classified as Cat 5). This event matches with the #5 position (February 10 1979) for the 10-day accumulated precipitation

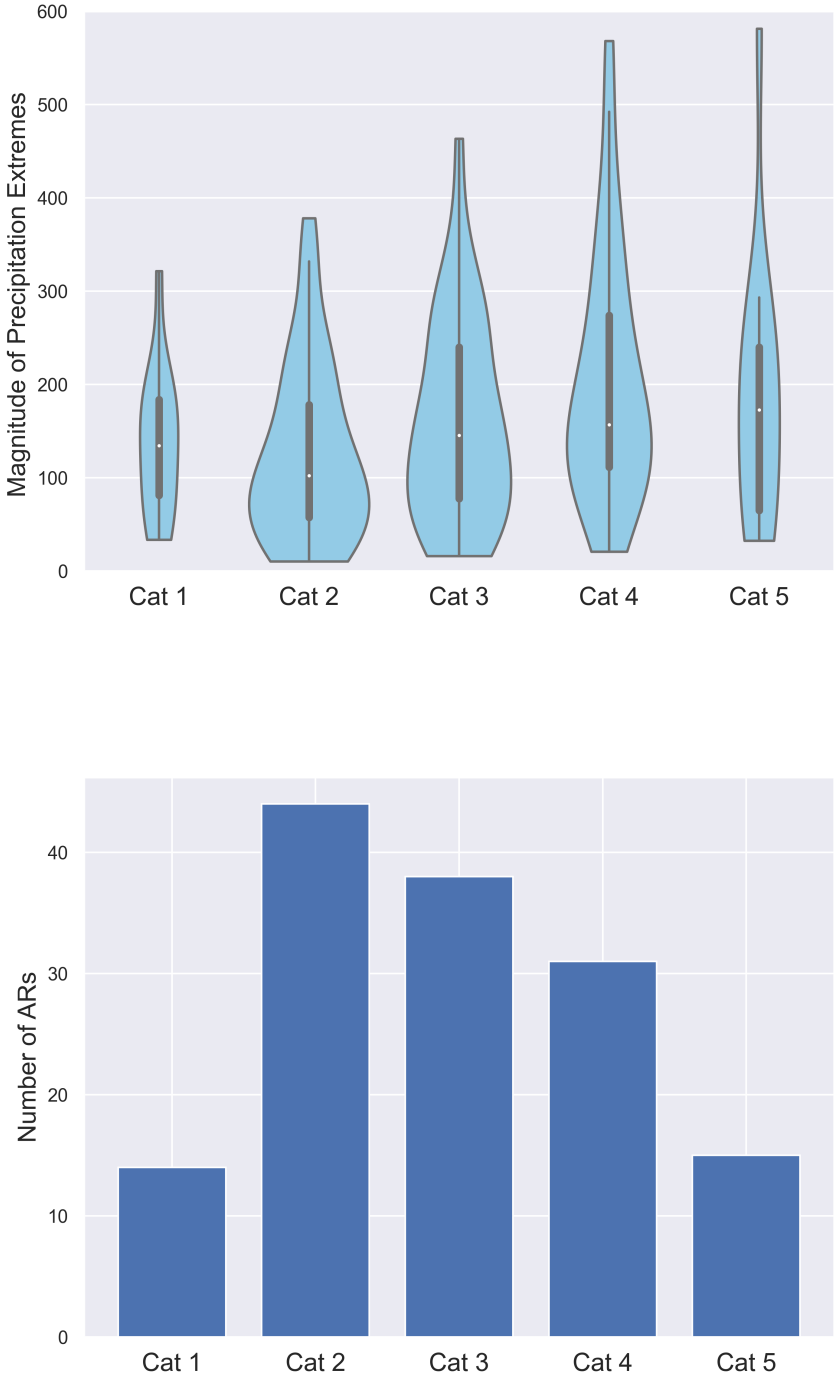

Figure 4.3: (top) Association between categorised Atmospheric Rivers (ARs) and 10-day accumulated precipitation ranking over IP. (bellow) Number of ARs in each Category.

extreme ranking over IP, with a magnitude equal to 581.36, as depicted in Table 2.1.

By solely considering ARs categorized as greater than Cat 1, and using information pertaining to the kernel distribution and quantile information, it is apparent that a discernible density distribution of the highest values of extreme precipitation exists as atmospheric rivers intensify. Despite the observed density distribution of extreme precipitation values corresponding to intensifying atmospheric rivers, the most extreme event (January 1970) for the 10-day accumulated precipitation ranking over IP does not

correspond to an AR. To gain insight into the underlying factors contributing to this precipitation extreme event, a specific analysis of the IVT and SLP fields during this period was conducted. Figure 4.4 shows that during 11 and 12 January 1970 there is clearly evidence of higher values of IVT (higher than 600 $\mathrm{kg\,m^{-1}\,s^{-1}}$), reaching almost 1400 $\mathrm{kg\,m^{-1}\,s^{-1}}$ over some areas along the North Atlantic within a transport directed eastwards, that reached the western part of IP, however with less intensity, during the January 11 afternoon extending into the night (Figure 4.4b, c, d). Despite these results, the automated detection algorithm does not consider this episode as an AR, as it does not satisfy the temporal and spatial requirements (section 3.1.2). The Figure 4.5 portrays the same representation as Figure 4.3, but this time for the 10-day accumulated precipitation ranking over Portugal. As with the IP analysis, results indicate that Cat 2, Cat 3, and cat 4 are the most frequent (Figure 4.5b). In a global context, the distribution shifts towards higher values as the AR classification increases, and the highest value for the magnitude of the precipitation extreme is 1046.30, which pertains to the #12 (February 10, 1979) position on the 10-day accumulated precipitation ranking over Portugal (Table 2.1). Similar to the findings for the IP results, this extreme precipitation event is associated with a Cat 5 AR that commenced on the 4 of February 1979 at 00:00 UTC, and attained significant intensity levels (exceeding 1000 $\mathrm{kg\,m^{-1}\,s^{-1}}$) in the region north of Portugal by 12:00 UTC (Figure 4.6a). After it arrived in the central region of the IP, the atmospheric river became stationary, while continuously being supplied with high levels of moisture from across the Atlantic (Figure 4.6b, c). This consistent moisture influx facilitated the AR persistence for a period of seven consecutive days, until the 10 of February (Figure 4.6d). The aforementioned representation enables us to provide a comprehensive description of the quality and quantity of this relationship. As the results align with the initial expectations, it can be concluded that the scale for ARs classification (Figure 4.1) is well-defined and the method helps to establish an objective link between the intensity of ARs and accumulated precipitation magnitudes (Figure 4.3 and Figure 4.5). As previously mentioned, it is possible to replicate similar outcomes for each river basin across IP.

However, in order to establish a stronger link between an AR event and a precipitation extreme event from the first ten ranking positions, it is necessary to examine a longer period of accumulated precipita-

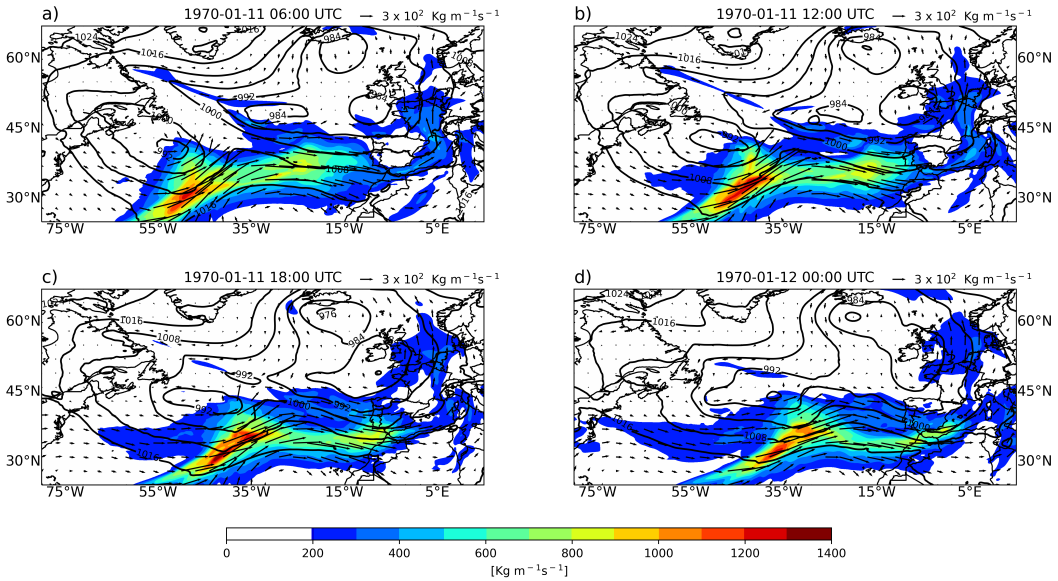

Figure 4.4: Integrated Water Vapor Transport (IVT) direction(vectors) and intensity ($\mathrm{kg\,m^{-1}\,s^{-1}}$; color shading) and SLP (hPA, contours) fields: (a) 1970-01-11 06:00 UTC; (b) 1970-01-11 12:00 UTC; (c) 1970-01-11 18:00 UTC; (d) 1970-01-12 00:00 UTC.

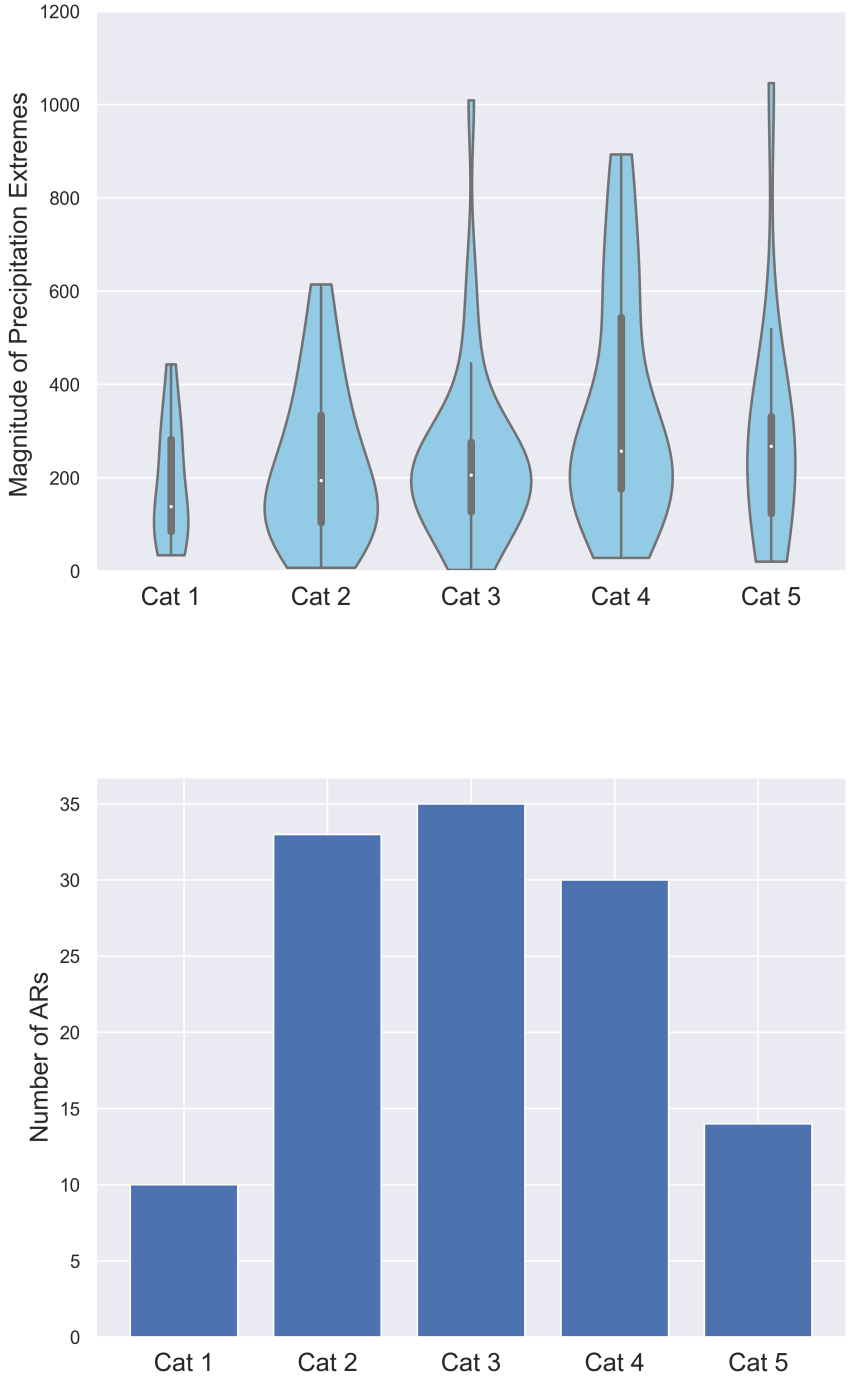

Figure 4.5: (top) Association between categorised Atmospheric Rivers (ARs) and 10-day accumulated precipitation ranking over Portugal. (bellow) Number of ARs in each Category.

tion. The findings indicate that, for Portugal, investigating the connection between an AR and extreme daily precipitation leads to a higher occurrence of matches with the top 10 precipitation extremes than for Iberia. Regarding the daily accumulated precipitation ranking over Portugal, the analysis revealed that six out of the top 10 positions were associated with an AR event. The highest value for the 10-day accumulated precipitation ranking over Portugal corresponded to the 12^{th} position (Not shown).
Based on the study's findings, it can be concluded that the Cat 4 AR that started on March 12 1969 at

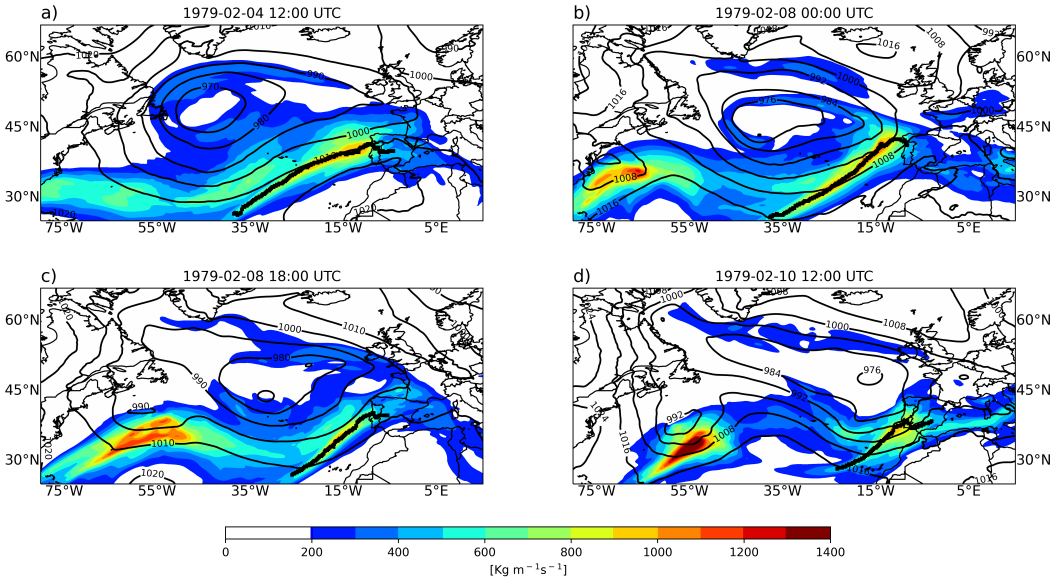

Figure 4.6: Integrated Water Vapor Transport (IVT) intensity ($\mathrm{kg\,m^{-1}\,s^{-1}}$; color shading) and SLP (hPA, contours) fields, and Atmospheric River core detected by the Algorithm (scatters) of a particular timestep: (a) 1979-02-04 12:00 UTC, (b) 1979-02-08 00:00 UTC, (c) 1979-02-08 18:00 UTC, (d) 1979-02-12 00:00 UTC

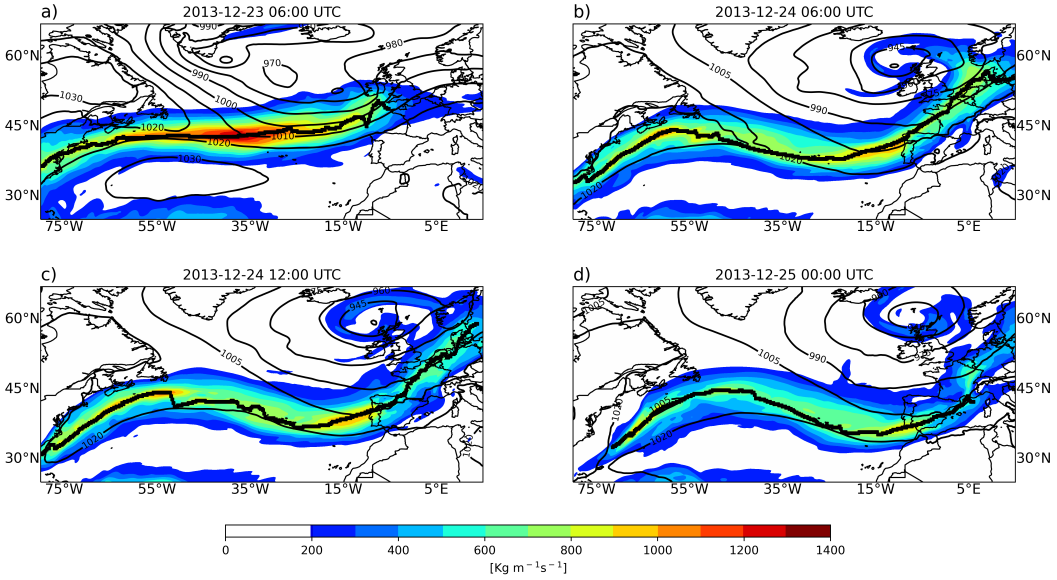

Figure 4.7: Integrated Water Vapor Transport (IVT) intensity ($\mathrm{kg\,m^{-1}\,s^{-1}}$; color shading) and SLP (hPA, contours) fields, and Atmospheric River core detected by the Algorithm (scatters) of a particular timestep: (a) 2013-12-23 06:00 UTC, (b) 2013-12-24 06:00 UTC, (c) 2013-12-24 12:00 UTC, (d) 2013-12-25 00:00 UTC

06:00 UTC and crossed Portugal primarily during the following 24 hours, ending on the 14 at 12:00 UTC, corresponds to the #1 ranked event in terms of daily accumulated period (March 12, 1969; Magnitude = 488) and 3-day (March 14 1969, Magnitude = 786.98) accumulated precipitation. It is important to emphasize that the most recent occurrence, falls within the top 10 for Portugal in terms of daily accumulated precipitation rank (the precipitation dataset only includes data up until 2015). This event, which occurred on 24 December 2013, ranks #7 in the precipitation ranking (daily scale) with a magnitude of 351.7. This extreme precipitation event was associated with a Cat 5 AR that began on December 23 at 06:00 UTC and had a predominantly meridian direction, affecting primarily the British Isles and the

French coast (Figure 4.7a). Interestingly, this particular AR displayed an uncommon behaviour, as it evolved southwards instead of progressing northwards. The AR reached Portugal at around 06:00 UTC on the 24 (Figure 4.7b), crossing the country until the end of the day (Figure 4.7c, d).

4.3 The impact of multiple ARs on the extreme precipitation events during December 2022

Many authors have shown, and the results presented here have confirmed, that extreme precipitation in the Western coasts of both Europe and USA is often triggered by ARs. The recent winter of 2022-2023 has underlined this evidence for both California and western Iberia, interestingly two regions widely affected by prolonged drought periods in recent years. Here it is shown that the significant transition from a dry period to an extremely wet one was largely influenced by the occurrence of multiple ARs impacting Iberia during December 2022. In fact, throughout December 2022, Portugal was struck by successive episodes of extreme precipitation, affecting a large part of the national territory, including the metropolitan regions of Lisbon and Porto (Gaspar et al., 2023). According to the climate bulletin provided by the Portuguese Institute of the Sea and the Atmosphere (IPMA), the month of December 2022 was classified as a very rainy month, with an average precipitation amount of 250.4 mm recorded, corresponding to 174% of the climatological normal value for the period of 1971-2000 (Instituto Português do Mar e da Atmosfera (IPMA), 2022). Of particular interest in the context of this work is the setting of new daily precipitation maxima observed in Lisbon between 9:00 am on the 12th and 9:00 am on the 13th December. This extreme precipitation event includes the absolute new maximum at the historical station of the Geophysical Institute in Lisbon, with over 150 years of continuous records, where 120.3 mm were recorded, surpassing the previous maximum observed in 2008 with 118.4 mm.

The detection scheme distinguished five independent ARs during December 2022. Therefore, based on the climatological analysis from 1959 to 2022, it can be concluded that December 2022 was an extremely anomalous month compared to the climatological results for the extended winter period with approximately 6 ARs per year.

Unfortunately, the precipitation that occurred during December 2022, is not available in the same grid as IB01 or IB02. Instead, IPMA provided precipitation data from 114 automated stations over mainland Portugal with a 10-minute temporal resolution. Therefore, the accumulated precipitation (hourly, daily, and over 3 days) was computed. A cubic interpolation (Wolber and Alfy, 1999) was also performed to interpolate values over all Portuguese territory instead of being confined to the marked point value at stations.

4.3.1 Results

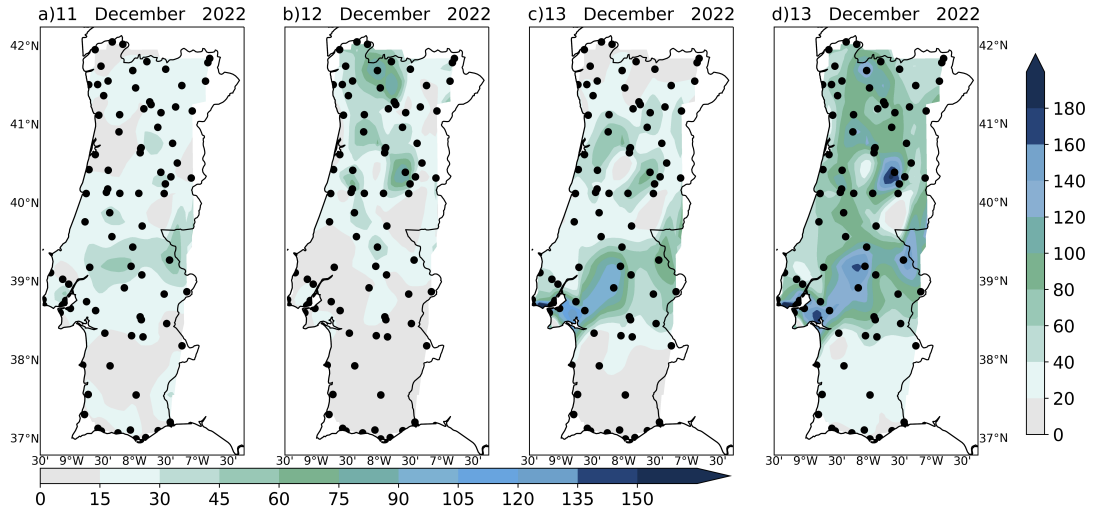

Figure 4.8: Daily precipitation (mm, shaded) for (a) December 11 2022, (b) December 12 2022, and (c) December 13 2022. (d) Accumulated precipitation (mm, shaded) between 11-13 December 2022. The black dots show the location of the 114 stations considered.

During December 2022, there were episodes of intense precipitation, particularly on days 4 and 5, 7 and 8, 12 and 13, and in the last days of the month, with flooding and overflowing occurring in various locations throughout the territory (Instituto Português do Mar e da Atmosfera (IPMA), 2022). In the two episodes of stronger precipitation (days 7-8 and 12-13), on average, according to IPMA, the total amount of precipitation related to these two episodes corresponded to about 50% of the total precipitation that occurred, over Portugal, during December 2022. For the sake of simplicity, the focus of the results will be on the extreme anomalous precipitation that occurred during the 11 -13 December period. Daily precipitation (mm) is presented in Figure 4.8a, b, c for the 11, 12, and 13 of December respectively. Overall, it was a persistent rainfall event, which was sometimes characterised by heavy rain in the North, Center, and Alto Alentejo regions, and in some locations in the Setúbal Peninsula. On December 11 (Figure 4.8a) intense precipitation occurred over a widespread area of the territory, reaching the highest values over the Central region (60mm). On December 12 (Figure 4.8b) the highest amount of precipitation occurred mainly over the Northern region, reaching the highest values (90mm), especially over Gerês, Braga, Vila-Real, and more to the South, Viseu. As previously mentioned, these days were characterised by the onset of an AR, starting on December 11 at 22:00 UTC. Figure 4.9a depicts the IVT intensity, SLP fields and the AR core of the event at 06:00 UTC when it made landfall over the northern region, and Figure 4.9b represents the total amount of precipitation between 05:00-06:00 UTC. Based on the data from the IPMA stations, it is known that no precipitation was recorded over Portugal until 05:00 UTC on December 12th. Therefore, it is reasonable to assume that it started to rain precisely at the same time as the eastern ending of the AR made landfall. By the end of the day, the atmospheric river crossed Portugal from North to South, with a decrease in intensity. Nevertheless, it still produced a significant impact with relatively intense precipitation mainly over Central and Northern regions (Figure 4.8b). Figure 4.8d represents the total rainfall amount for the 11-13 December period, confirming that high values were recorded over the north and central sectors of Portugal. The record values obtained for these 3 days

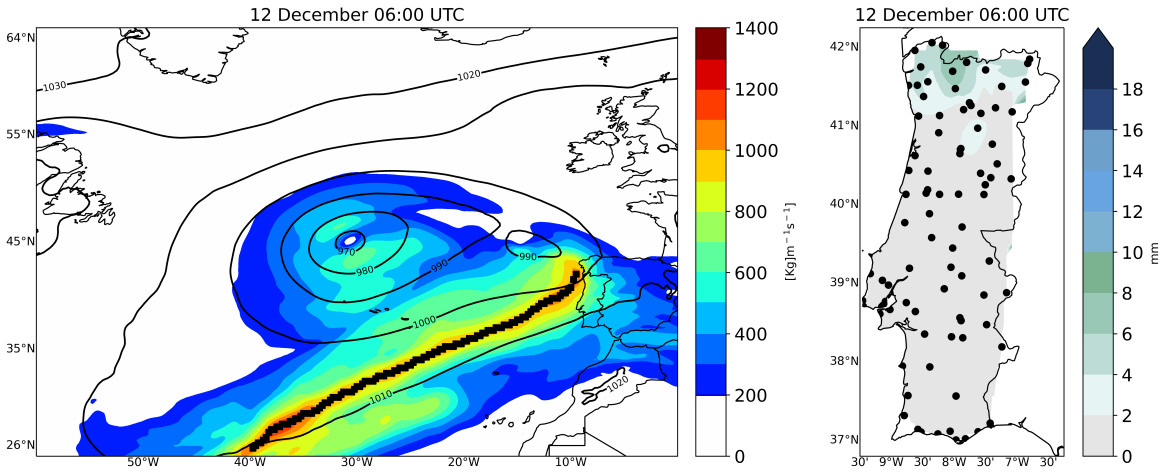

Figure 4.9: (a) Integrated Water Vapor Transport (IVT) intensity ($\mathrm{kg\,m^{-1}\,s^{-1}}$), SLP (hPa; contours) fields, and Atmospheric River core detected by the Algorithm (scatters); (b) Hourly precipitation (mm, shaded) for 12 December at 06:00 UTC.

were observed in Lisboa/IPMA (168.1 mm), Lisboa/Alges (147.9 mm), and Alentejo/Mora (137.8 mm) stations. The extreme precipitation that occurred in Lisbon and was responsible for high socioeconomic losses due to floodings and urban inundations, mostly occurred in the early morning of 13 December. In fact, according to our results, in the early morning (05:00 UTC), an intensification was observed on the IVT field reaching the Portuguese coast, advected from the Atlantic Ocean (Figure 4.10a).

This intense and channelled IVT was responsible for an extreme amount of precipitation (rainfall rates higher than 12 mm/h during several hours) over Lisbon and Alto Alentejo regions (Figure 4.10b). After performing a detailed analysis of precipitation extremes in a climatological mode (period 1950-2015), the daily precipitation mean climatological value and respective daily STD value were obtained for a

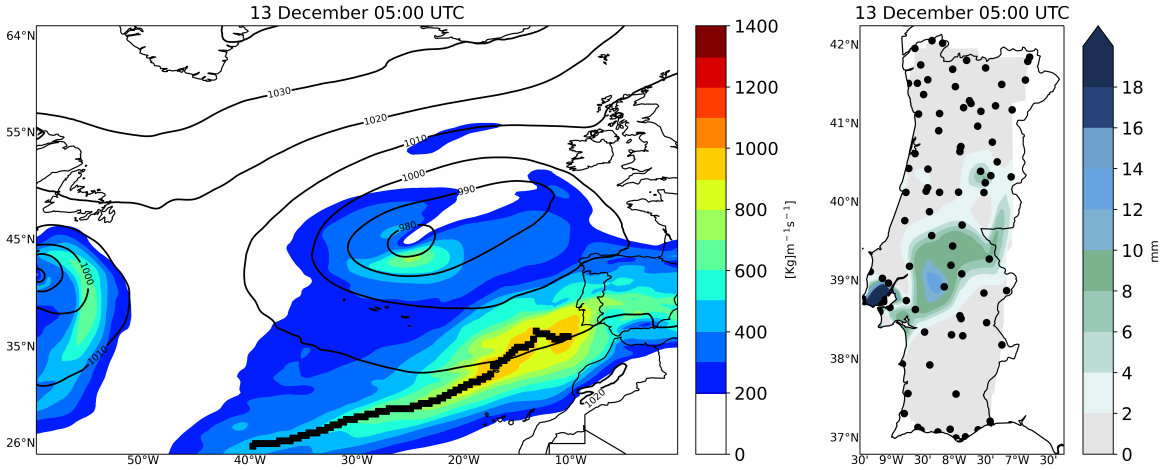

Figure 4.10: (a) Integrated Water Vapor Transport (IVT) intensity ($\mathrm{kg\,m^{-1}\,s^{-1}}$, SLP (hPa; contours) fields, and Atmospheric River core detected by the Algorithm (scatters); (b) Hourly precipitation (mm, shaded) for 13 December at 05:00 UTC.

particular Julian day and each grid point over the IP with a 0.1º spatial resolution. Considering this, the grid cells that include each one of the 114 stations were selected in an attempt to merge these climatological gridded results with the precipitation dataset for December 2022. Then, the normalized precipitation anomalies (N) were computed for all the 114 station locations. For the sake of simplicity, the results for the 3 stations referred above are presented: it can be concluded that the Lisboa/Algés station attained a precipitation amount (147.9 mm) that was 12.5 STD above the climatological value; the Lisboa/IPMA (168.1mm) and the Alentejo/Mora (137.8 mm) stations were, respectively, at 14.5 and 13 STD above its climatological values.
Considering these specific results from stations and the analysis of this extreme precipitation episode, it can be confidently expected that, when the data becomes available on a regular grid similar to the IB01 or IB02 datasets and the magnitude of this episode (as described in the previous section) is calculated, this event will almost certainly rank very high in the multi-day extreme precipitation rankings, particularly over Portugal.

4.4 Summary

The most important results obtained in this chapter can be summarized as follows:

- The ARs were classified based on the mean IVT values along the AR core during the persistent event and the duration of the event at a given location, following a categorization approach developed by Ralph (2018). By doing so, the study aimed to quantify and determine the extent to which large rainfall amounts are linked to the presence of ARs in the North Atlantic region.

- The study investigates the association between extreme precipitation days and ARs for the entire IP and seven smaller subdomains as previously defined (Ramos et al. 2014). The highest positions in various precipitation ranks often coincide with AR occurrences, with a more pronounced impact in northern domains compared to southern domains.

- The contribution of ARs to extreme precipitation events exhibits significant variability across ranking positions. For most regions, this contribution decreases notably from the highest to the lowest extreme days.

- This section also analyzed in detail the extremely anomalous month of December 2022 in terms of precipitation and the possible role played by ARs. There were several episodes of intense precipitation throughout the month, particularly on the 4 and 5, 7 and 8, 12 and 13, and also during the last few days of the month, which resulted in flooding and overflowing in various locations throughout the territory.

- Obtained results allow us to conclude that, during the most intense event during the days 11, 12, and 13, repeated episodes of heavy precipitation gave rise to several flash floods in various urban areas, especially in the Greater Lisbon area and also some regions of Alto Alentejo. Both the areas affected, and the timing of occurrence, match almost perfectly with the passage of a strong AR.

- New daily precipitation maximum records were set on December 13 in several stations of Lisbon and Alentejo.

- The study concludes that ARs are a significant contributor to extreme precipitation events in the IP, and their potential impact should be considered when assessing and managing the risks associated

with these events. The results also emphasize the importance of analyzing different subdomains and time scales to better understand the spatial and temporal variability of extreme precipitation events associated with ARs.

Chapter 5

Conclusions

Atmospheric Rivers (ARs) are responsible for over 90% of poleward water vapor transport in the mid-latitudes and can produce extreme precipitation when making landfall (Liu et al., 2021). Moisture transport, particularly through ARs, plays a key role in extreme precipitation events in Western Europe (Ramos et al., 2015; Lavers and Villarini, 2013). Consequently, ARs have garnered increasing interest among scientists, policymakers, and the public due to their impact on water resources, climate variability, and extreme weather events. Given the importance of the ARs in the extreme precipitation in the Iberian peninsula, it is important to remind the main objectives of this work:

- To create a comprehensive database of extreme precipitation events for the Iberian Peninsula, covering various time scales (1 to 10 days) from 1950 to 2015. Utilizing two precipitation datasets (Iberia 01 and Iberia 02) and adopting the methodology from Ramos (2016), the research develops objective rankings for extreme precipitation events developed for the entire Iberian Peninsula, Portugal, and major regional river basins, focusing on the extended winter season (October to March). Notably, the analysis reveals that certain short-term extreme events may not rank high in longer time scales, and top events in one river basin often do not appear in neighbouring basin rankings, irrespective of the time frame. It is important to highlight that the results are purely based on statistical estimation and lack an assessment of the physical mechanisms behind these extreme episodes.

- The second objective of the work was to identify the ARs that affected the Iberian Peninsula (IP) over the 1959–2022 period during the extended winter months. To achieve this, the same approach as Ramos (2015) was followed, applying an automated ARs detection algorithm to western Iberia using ERA-5 reanalysis datasets (as explained in detail in section 3.1). After identifying ARs and analyzing their characteristics such as length, duration, and intensity, the focus was on the circulation patterns associated with these events.

- The last main objective of this investigation focused on assessing the impact of ARs on extreme precipitation events. AR events were categorized based on Ralph's (2019) work, detailed in section 4.1. The study evaluated the appropriateness of the classification scale by establishing a link between AR categories and the magnitude of associated precipitation extremes. Existing literature suggests a connection between AR landfall and extreme precipitation events (Gaspar et al., 2023; Ralph et al., 2019; Ramos et al., 2015; Lavers and Villarini, 2013), and the study aimed to quantitatively and qualitatively evaluate this relationship.

In this regard, a systematic approach was presented for evaluating extreme precipitation periods in

the IP region through the analysis of multi-day accumulated precipitation anomalies over varying time scales between 1 and 10 days. This method considers the daily precipitation anomalies and emphasizes the significance of anomalies over daily, 3, 5, 7, and 10-day periods. The magnitude of a precipitation episode is given considering the area (in percentage) that has precipitation anomalies above two standard deviations (STD) and also the mean values of these anomalies over this area. The method defines an anomalous precipitation "case" as an n-day period of accumulated precipitation, which is ranked based on its anomalous intensity. An anomalous precipitation "event" is identified as a group of cases with an anomalous intensity that occurs either in the same or different rankings of accumulated precipitation periods. The method used followed the steps of the first complete assessment of daily precipitation ranking days in the IP (Ramos et al., 2016; Ramos et al., 2014). But while the gridded precipitation dataset used in those works ended in 2008 and had a 0.2ºX 0.2º latitude/longitude resolution (IB02; Belo-Pereira et al., 2011; Herrera et al., 2010), here a longer time series, ending in 2015 and with higher resolution (0.1ºX 0.1º latitude/longitude; Herrera et al., 2019) was used. The methodology was applied to assess extreme precipitation periods across the entire IP region and in specific domains such as Portugal and the six major river basins in the IP, namely Minho, Duero, Tagus, Guadiana, Guadalquivir, and Ebro. Through several representative examples, the study has allowed some noteworthy observations. Firstly, the methodology developed for computing daily rankings was confirmed to be useful for studying multi-day accumulated precipitation rankings across the eight different domains considered. Secondly, the rankings databases generated for the various domains and time scales can prove to be valuable for other studies aimed at comprehending the causes and consequences of extreme precipitation events occurring over large areas. This includes hydrologists, water resource managers, and insurers of socio-economic activities like agriculture and hydroelectricity production. Thirdly, it was observed that for the different domains, a few extreme precipitation events dominate the top ten rankings. This can be attributed to the analysis of successive accumulated precipitation days over relatively long periods. Fourthly, the top ten precipitation episodes for the six different river basins are largely non-coincident, underscoring the strong spatial variability of extreme precipitation phenomena in the IP. Finally, the methodology employed to construct the rankings allows for a distinct analysis of extreme events based on high precipitation totals, extensive areas affected by less extreme precipitation values, or persistent rainy conditions over longer periods.

Regarding the second objective, in order to identify the ARs that impacted the IP, the Integrated Vapor Transport (IVT) approach was used, following the methodology established by Ramos et al., (2015). The state-of-the-art ERA-5 reanalysis data spanning from 1959 to 2022 was used for this purpose. The analysis results can be summarized as follows: the study identified an average of 6 atmospheric rivers per extended winter period between 1959-2022 using ERA-5 data. The number of ARs per month decreases after December, with 85 ARs detected during that month, but less than 30 in March. The majority of the ARs (190, or 52.5%) lasted less than 24 hours, and their length was found to fall between 2040 and 3360 km. For the persistent AR time steps, negative anomalies of sea level pressure (SLP) were observed around Ireland, while positive anomalies were present over northern Africa. This SLP gradient configuration is consistent with a strong wind field that induces the rapid transport of moisture towards the Iberian Peninsula, which is closely associated with the AR. These findings are consistent with those of Lavers and Villarini (2013; 2012) and Ramos et al (2015), who studied the impact of ARs over coastal regions in Europe, particularly the Iberian Peninsula. The configuration of the SLP gradient supports the occurrence of ARs in the Iberian Peninsula, and its correlation with the EA large-scale circulation pattern is stronger than with other modes of variability such as the NAO or SCAND, which have a relatively weaker influence. The purpose of the final part of this study was to assess the relationship

between ARs and multi-day precipitation extreme events in the IP. To achieve this, the AR events were classified based on the maximum instantaneous IVT and the duration of the event at a given location, following a categorization approach developed by Ralph (2018). The ARs were classified based on the mean IVT values along the AR core during the persistent event. By doing so, the study aimed to quantify and determine the extent to which large rainfall amounts are linked to the presence of ARs in the North Atlantic region from 1959 to 2015, which was common to both datasets. In this regard, the study yielded several conclusions: It was found that ARs are more significant in the northern domains of the IP compared to the southern domains and are often associated with the highest positions in various precipitation ranks. The occurrence of extreme precipitation days is highly sensitive to the latitudinal location of the ARs associated with different subdomains, given the narrow nature of the ARs. Finally, a case study of one of the most extreme precipitation days over the IP and Portugal that occurred from 11 to 13 December 2022 was analyzed, and it was found that the large-scale atmospheric flow associated with these extreme rainfall and flash flood episodes on the IP resulted from the simultaneous occurrence of favourable thermodynamic conditions, including the presence of an AR structure which was classified as a category 5. The AR commenced on the 12th of December and attained significant intensity levels (exceeding 1000 $\mathrm{kg, m^{-1}, s^{-1}}$) in the northern region of Portugal by 12:00 UTC. Subsequent to its arrival in the central region of the IP, the AR became stationary, while continuously being supplied with high levels of moisture from across the Atlantic.

After this study, it is clear that ARs represent a significant contributor to extreme precipitation events in the IP, and their potential impact should be considered when assessing and managing the risks associated with these events. The results also emphasize the importance of analyzing different subdomains and time scales to better understand the spatial and temporal variability of extreme precipitation events associated with ARs.

Appendix A

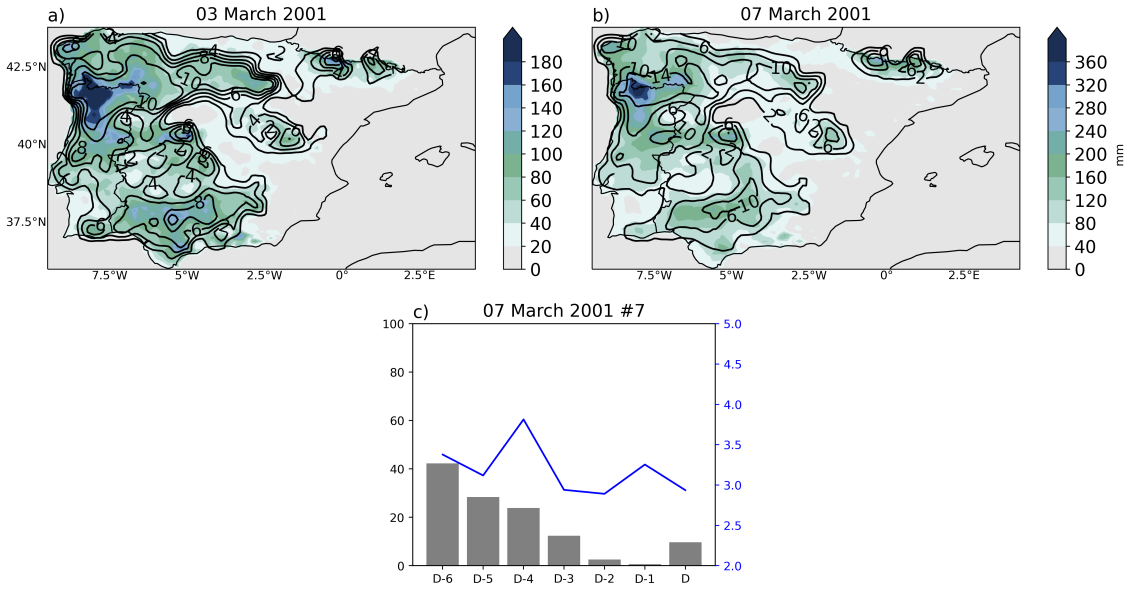

Figure A.1: Three days accumulated precipitation (mm, shaded) and corresponding standard deviation anomalies (black contour) of the first most anomalous (3 days ranking) case in the Iberian Peninsula – 3 March 2001, (b) 7 days accumulated precipitation (mm, shaded) and corresponding standard deviation anomalies (black contour) of the #7 (7 days ranking) case in Iberian Peninsula – 7 March 2001. (c) The percentage of area above the 2 std (bars) and the respective anomaly mean (blue line) between 1 March and 7 March 2001 is also shown for the Iberian Peninsula domain.

Table A.1: The ten most anomalous precipitation cases for each river basin and regarding the 10 days accumulated period.

#Ranking	Minho	Duero	Tagus	Guadiana	Guadalquivir	Ebro
1	14 Feb 1979	31 Dec 1995	11 Jan 1970	11 Jan 1970	30 Dec 2009	26 Oct 2012
2	13 Feb 1979	13 Feb 1979	09 Feb 1972	29 Dec 2009	29 Dec 2009	27 Oct 2012
3	15 Dec 1978	20 Feb 1966	12 Jan 1970	30 Dec 2009	27 Dec 2009	06 Feb 2015
4	10 Feb 1979	01 Jan 1996	08 Feb 1972	21 Dec 1958	26 Dec 2009	07 Feb 2015
5	12 Feb 1979	30 Dec 1995	07 Feb 1972	05 Jan 1963	05 Jan 1963	05 Feb 2015
6	11 Feb 1979	21 Feb 1966	06 Feb 1972	12 Jan 1970	25 Dec 2009	08 Feb 2015
7	16 Dec 1978	18 Feb 1966	10 Jan 1970	22 Dec 1958	28 Dec 2009	17 Nov 1967
8	15 Feb 1979	14 Feb 1979	13 Jan 1970	10 Jan 1970	11 Jan 1970	26 Mar 1974
9	30 Nov 1952	12 Feb 1979	05 Feb 1972	04 Jan 1963	04 Jan 1963	28 Mar 1974
10	31 Dec 1978	10 Feb 1979	30 Dec 1981	26 Nov 1989	12 Jan 1970	27 Mar 1974

A.

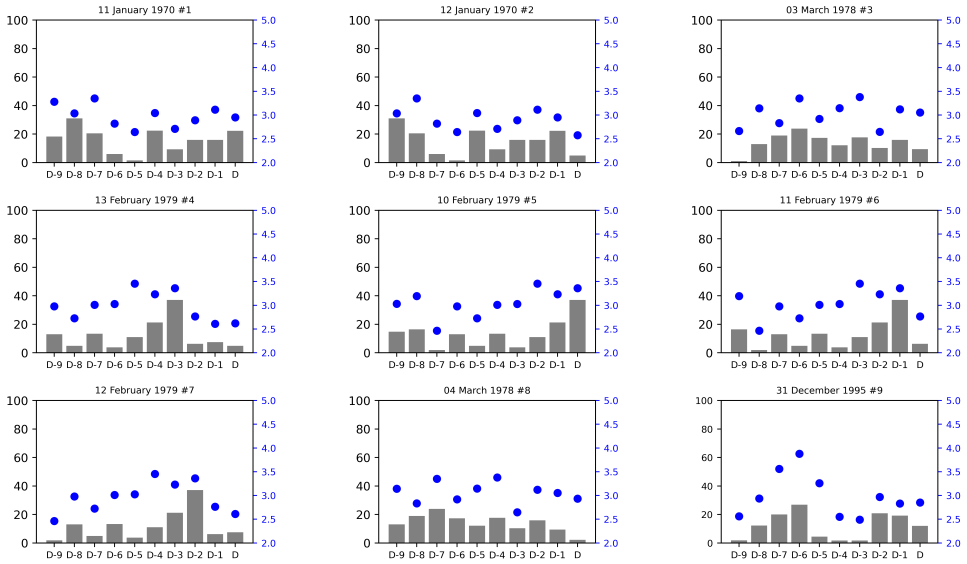

Figure A.2: The percentage of Area above the 2std (bars) and the respective average anomaly (blue line) for the Iberian Peninsula domain for the top 9 of the 10 days accumulated ranking.

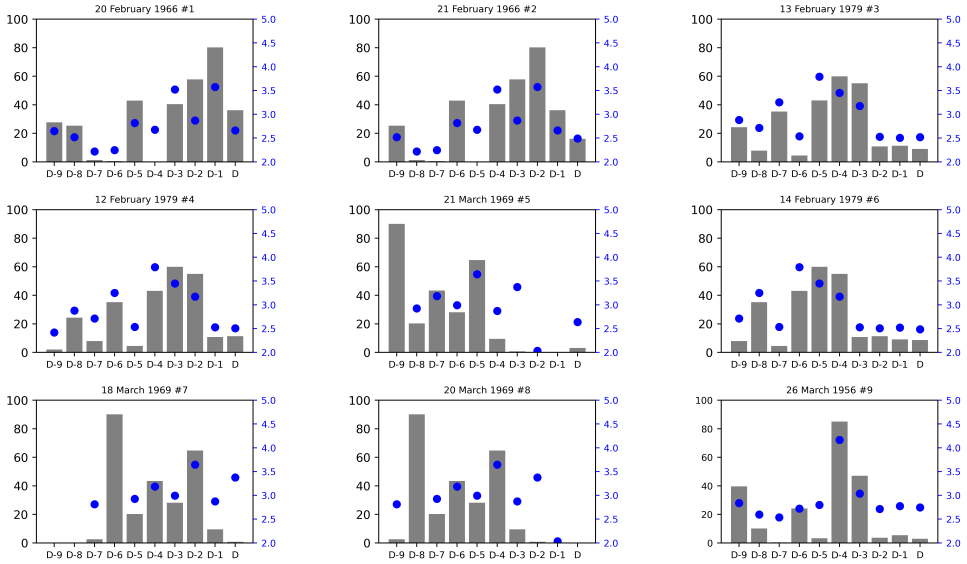

Figure A.3: The percentage of Area above the 2std (bars) and the respective average anomaly (blue line) for the Portugal domain for the top 9 of the 10 days accumulated ranking.

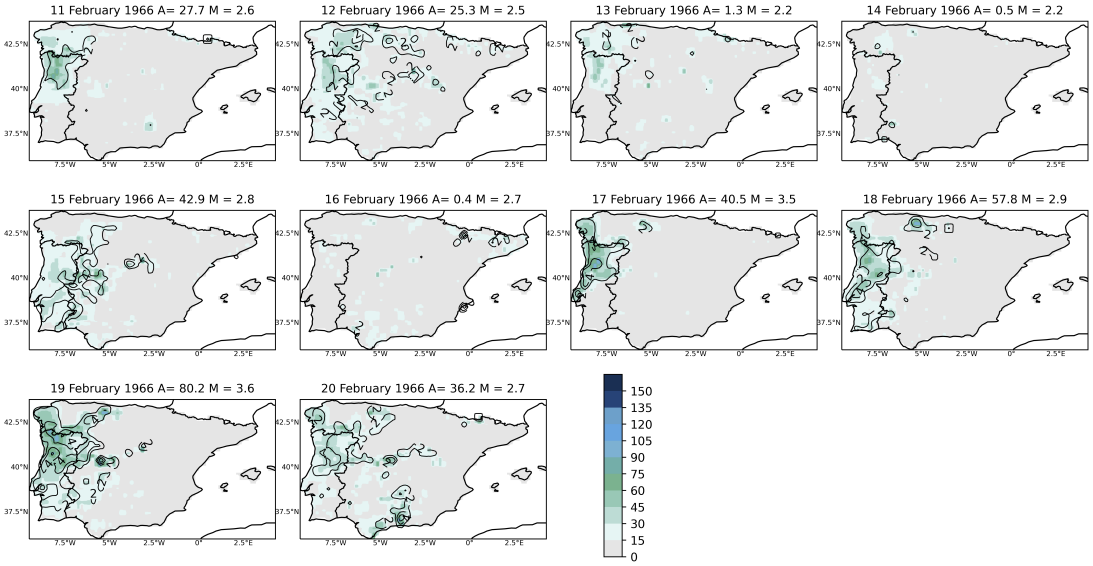

Figure A.4: Daily precipitation (mm, shaded) and corresponding standard deviation anomalies (black contour) between 11 February 1966 and 20 February 1966 of the most extreme case for the 10-day accumulated period over the Portuguese domain.

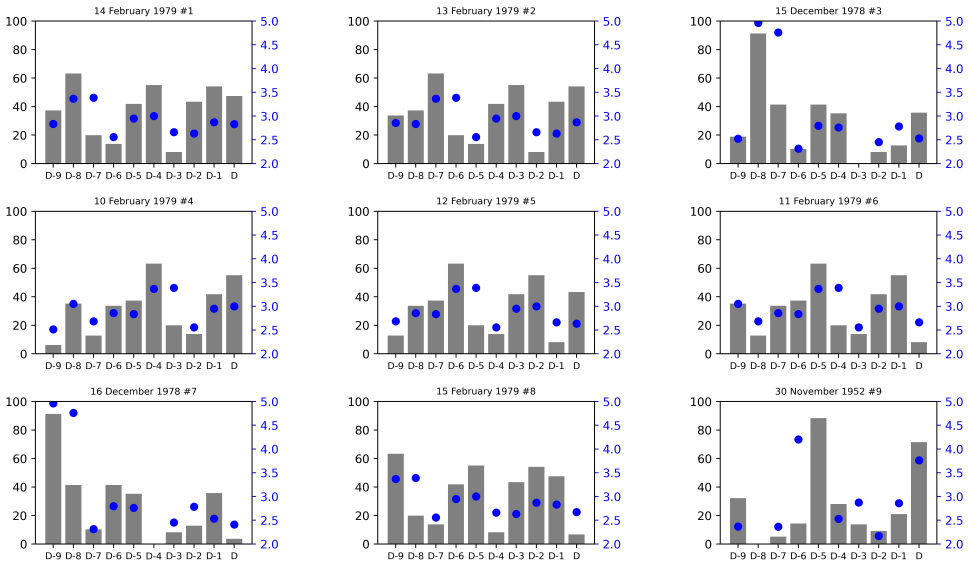

Figure A.5: The percentage of Area above the 2std (bars) and the respective average anomaly (blue line) for the Minho domain for the top 9 of the 10 days accumulated ranking.

A.

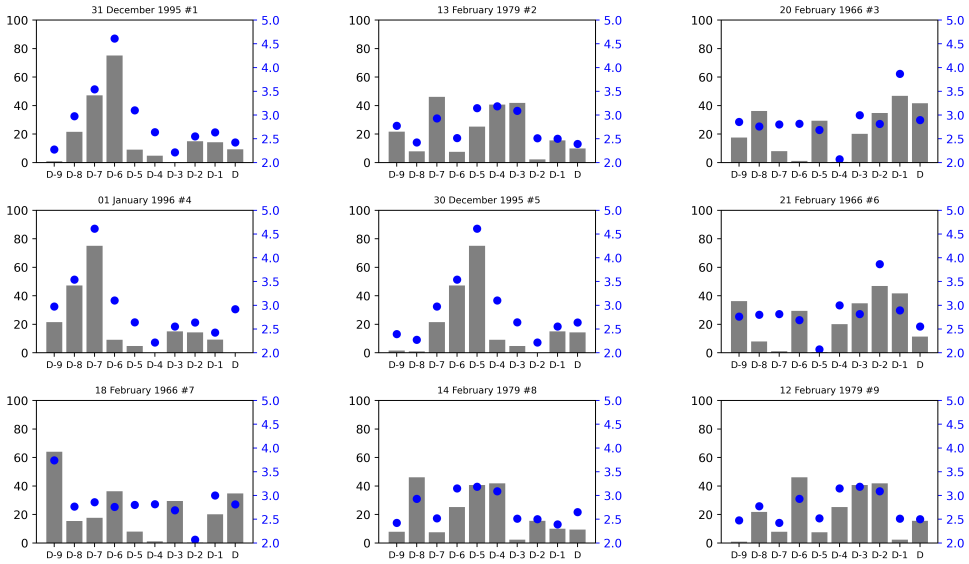

Figure A.6: The percentage of Area above the 2std (bars) and the respective average anomaly (blue line) for the Duero domain for the top 9 of the 10 days accumulated ranking.

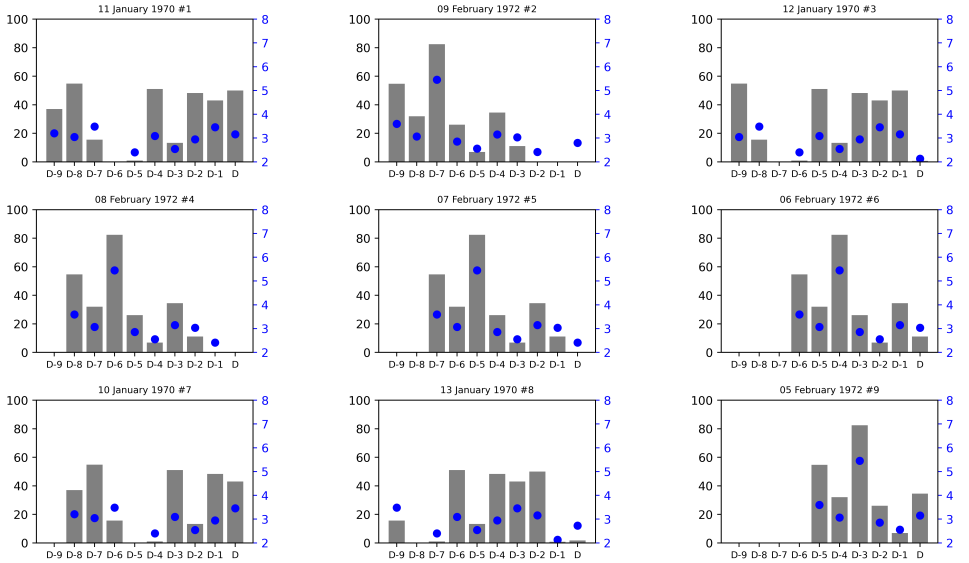

Figure A.7: The percentage of Area above the 2std (bars) and the respective average anomaly (blue line) for the Tagus domain for the top 9 of the 10 days accumulated ranking.

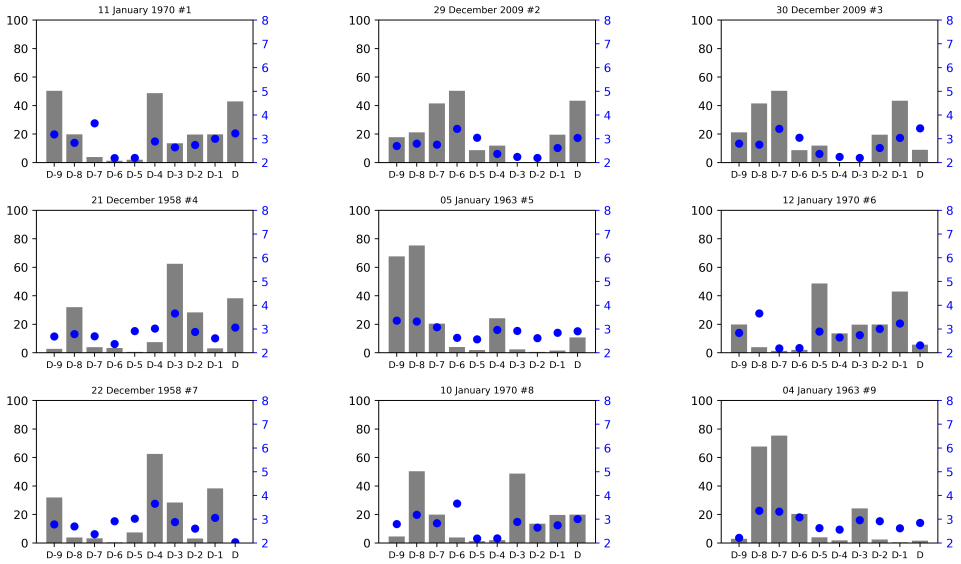

Figure A.8: The percentage of Area above the 2 std (bars) and the respective average anomaly (blue line) for the Guadiana domain for the top 9 of the 10 days accumulated ranking.

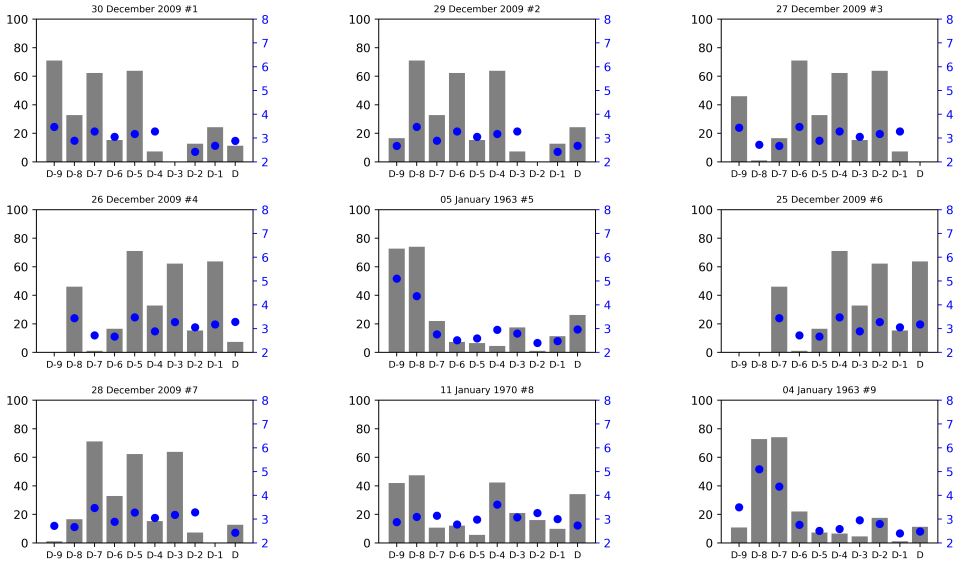

Figure A.9: The percentage of Area above the 2std (bars) and the respective average anomaly (blue line) for the Guadalquivir domain for the top 9 of the 10 days accumulated ranking.

A.

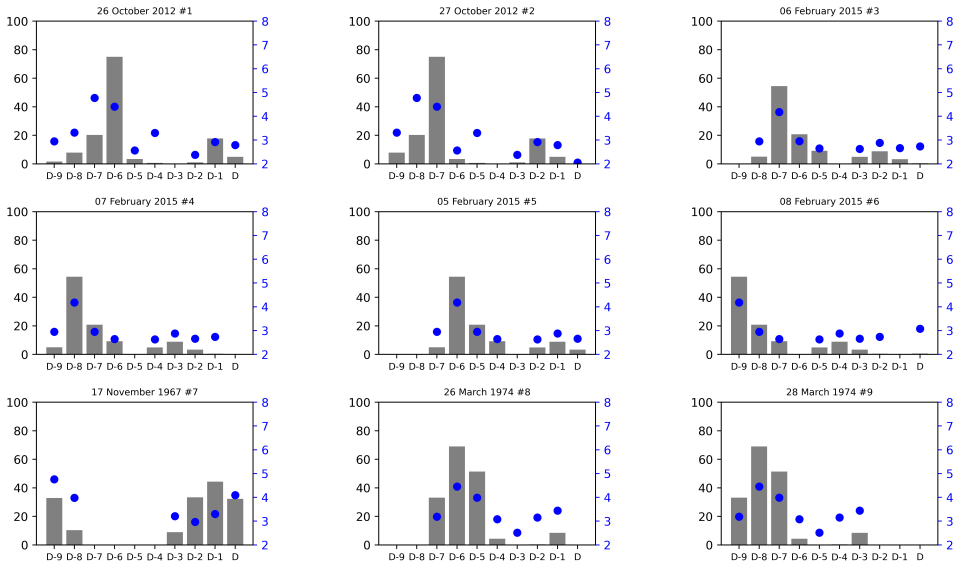

Figure A.10: The percentage of Area above the 2std (bars) and the respective average anomaly (blue line) for the Ebro domain for the top 9 of the 10 days accumulated ranking.

Bibliography

Bao, J., Michelson, S., Neiman, P., Ralph, F., & Wilczak, J. (2006). Interpretation of enhanced integrated water vapor bands associated with extratropical cyclones: Their formation and connection to tropical moisture. *Monthly weather review*, *134*(4), 1063–1080.

Barnston, A. G., & Livezey, R. E. (1987). Classification, seasonality and persistence of low-frequency atmospheric circulation patterns. *Monthly weather review*, *115*(6), 1083–1126.

Belo-Pereira, M., Dutra, E., & Viterbo, P. (2011). Evaluation of global precipitation data sets over the iberian peninsula. *Journal of Geophysical Research*, *116*. https://doi.org/10.1029/2010jd015481

Brands, S., Gutiérrez, J., & San-Martin, D. (2017). Twentieth-century atmospheric river activity along the west coasts of europe and north america: Algorithm formulation, reanalysis uncertainty and links to atmospheric circulation patterns. *Climate Dynamics*, *48*, 2771–2795. https://doi.org/10.1007/s00382-016-3095-6

Cardoso, R. M., Soares, P. M., Lima, D. C., & Miranda, P. M. (2019). Mean and extreme temperatures in a warming climate: Euro cordex and wrf regional climate high-resolution projections for portugal. *Climate Dynamics*, *52*, 129–157.

Cardoso Pereira, S., Marta-Almeida, M., Carvalho, A. C., & Rocha, A. (2019). Extreme precipitation events under climate change in the iberian peninsula. *International Journal of Climatology*, *40*, 1255–1278. https://doi.org/10.1002/joc.6269

Casanueva, A., Rodríguez-Puebla, C., Frías, M., & González-Reviriego, N. (2014). Variability of extreme precipitation over europe and its relationships with teleconnection patterns. *Hydrology and Earth System Sciences*, *18*(2), 709–725.

Cortesi, N., Gonzalez-Hidalgo, J. C., Trigo, R. M., & Ramos, A. M. (2013). Weather types and spatial variability of precipitation in the iberian peninsula. *International Journal of Climatology*, *34*, 2661–2677. https://doi.org/10.1002/joc.3866

De Lima, M. I. P., Santo, F. E., Ramos, A. M., & de Lima, J. L. (2013). Recent changes in daily precipitation and surface air temperature extremes in mainland portugal, in the period 1941–2007. *Atmospheric Research*, *127*, 195–209.

De Lima, M. I. P., Santo, F. E., Ramos, A. M., & Trigo, R. M. (2015). Trends and correlations in annual extreme precipitation indices for mainland portugal, 1941–2007. *Theoretical and Applied Climatology*, *119*, 55–75.

Eiras-Barca, J., Lorenzo, N., Taboada, J., Robles, A., & Miguez-Macho, G. (2018). On the relationship between atmospheric rivers, weather types and floods in galicia (nw spain). *Natural hazards and earth system sciences*, *18*(6), 1633–1645.

Eiras-Barca, J., Ramos, A. M., Algarra, I., Vázquez, M., Dominguez, F., Miguez-Macho, G., Nieto, R., Gimeno, L., Taboada, J., & Ralph, F. M. (2021). European west coast atmospheric rivers: A scale to characterize strength and impacts. *Weather and Climate Extremes*, *31*, 100305. https://doi.org/10.1016/j.wace.2021.100305

BIBLIOGRAPHY

Garaboa-Paz, D., Eiras-Barca, J., Huhn, F., & Pérez-Muñuzuri, V. (2015). Lagrangian coherent structures along atmospheric rivers. *Chaos: An Interdisciplinary Journal of Nonlinear Science*, *25*(6).

García-Herrera, R., Hernández, E., Barriopedro, D., Paredes, D., Trigo, R. M., Trigo, I. F., & Mendes, M. A. (2007). The outstanding 2004/05 drought in the iberian peninsula: Associated atmospheric circulation. *Journal of Hydrometeorology*, *8*, 483–498. https://doi.org/10.1175/jhm578.1

Gaspar, T., Ramos, A. M., Deus, R., Pinto, P. J., & Trigo, R. M. (2023). The impact of multiple atmospheric rivers on the extreme precipitation events in december 2022 in portugal. *Meteorology and Geophysics*, 52.

Gimeno, L., Nieto, R., Vázquez, M., & Lavers, D. A. (2014). Atmospheric rivers: A mini-review. *Frontiers in Earth Science*, *2*, 2.

Gimeno, L., Stohl, A., Trigo, R. M., Dominguez, F., Yoshimura, K., Yu, L., Drumond, A., Durán-Quesada, A. M., & Nieto, R. (2012). Oceanic and terrestrial sources of continental precipitation. *Reviews of Geophysics*, *50*. https://doi.org/10.1029/2012rg000389

Herrera, S., Gutiérrez, J. M., Ancell, R., Pons, M. R., Frías, M. D., & Fernández, J. (2010). Development and analysis of a 50-year high-resolution daily gridded precipitation dataset over spain (spain02). *International Journal of Climatology*, *32*, 74–85. https://doi.org/10.1002/joc.2256

Herrera, S., Cardoso, R. M., Soares, P. M., Espírito-Santo, F., Viterbo, P., & Gutiérrez, J. M. (2019). Iberia01: A new gridded dataset of daily precipitation and temperatures over iberia. *Earth System Science Data*, *11*, 1947–1956. https://doi.org/10.5194/essd-11-1947-2019

Instituto Português do Mar e da Atmosfera (IPMA). (2022). *Ipma climate report*. https://www.ipma.pt/pt/media/noticias/documentos/2022/Boletim_clima_IPMA_dez2022.pdf

Knippertz, P., & Wernli, H. (2010). A lagrangian climatology of tropical moisture exports to the northern hemispheric extratropics. *Journal of Climate*, *23*(4), 987–1003.

Lavers, D. A., & Villarini, G. (2013). The nexus between atmospheric rivers and extreme precipitation across europe. *Geophysical Research Letters*, *40*, 3259–3264. https://doi.org/10.1002/grl.50636

Lavers, D. A., Villarini, G., Allan, R. P., Wood, E. F., & Wade, A. J. (2012). The detection of atmospheric rivers in atmospheric reanalyses and their links to british winter floods and the large-scale climatic circulation. *Journal of Geophysical Research: Atmospheres*, *117*. https://doi.org/10.1029/2012jd018027

Leung, L. R., & Qian, Y. (2009). Atmospheric rivers induced heavy precipitation and flooding in the western u.s. simulated by the wrf regional climate model. *Geophysical Research Letters*, *36*, n/a–n/a. https://doi.org/10.1029/2008gl036445

Liberato, M. L. R., Ramos, A. M., Trigo, R. M., Trigo, I. F., Durán-Quesada, A. M., Nieto, R., & Gimeno, L. (2013). Moisture sources and large-scale dynamics associated with a flash flood event. *Lagrangian Modeling of the Atmosphere*, 111–126. https://doi.org/10.1029/2012gm001244

Lionello, P., Abrantes, F., Congedi, L., Dulac, F., Gacic, M., Gomis, D., Goodess, C., Hoff, H., Kutiel, H., Luterbacher, J., Planton, S., Reale, M., Schröder, K., Vittoria Struglia, M., Toreti, A., Tsimplis, M., Ulbrich, U., & Xoplaki, E. (2012). Introduction: Mediterranean climate—background information. *The Climate of the Mediterranean Region*, xxxv–xc. https://doi.org/10.1016/b978-0-12-416042-2.00012-4

Liu, X., Ma, X., Chang, P., Jia, Y., Fu, D., Xu, G., Wu, L., Saravanan, R., & Patricola, C. M. (2021). Ocean fronts and eddies force atmospheric rivers and heavy precipitation in western north america. *Nature Communications*, *12*. https://doi.org/10.1038/s41467-021-21504-w

Martin-Vide, J., & Gil Olcina, J. (2001). Tiempos y climas de españa. *Madrid, Alianza Editorial. Col. El libro universitario*.

Moon, K.-W. (2016). Violin plot. In *Learn ggplot2 using shiny app* (pp. 191–200). Springer International Publishing. https://doi.org/10.1007/978-3-319-53019-2_20

Neiman, P. J., Ralph, F. M., Wick, G. A., Lundquist, J. D., & Dettinger, M. D. (2008). Meteorological characteristics and overland precipitation impacts of atmospheric rivers affecting the west coast of north america based on eight years of ssm/i satellite observations. *Journal of Hydrometeorology*, *9*, 22–47. https://doi.org/10.1175/2007jhm855.1

Newell, R. E., Newell, N. E., Zhu, Y., & Scott, C. (1992). Tropospheric rivers?–a pilot study. *Geophysical research letters*, *19*(24), 2401–2404.

Peixoto, J. P., & Oort, A. H. (1992). *Physics of climate*. American Institute Of Physics.

Ralph, F. M., & Dettinger, M. D. (2011). Storms, floods, and the science of atmospheric rivers. *Eos, Transactions American Geophysical Union*, *92*, 265–266. https://doi.org/10.1029/2011eo320001

Ralph, F. M., Dettinger, M. D., Rutz, J. J., Waliser, D. E., & Bosart, L. F. (2020). *Atmospheric rivers*. Springer.
Atmospheric River Modeling: Forecasts, Climate Simulations, And Climate Projections. Ch. 3.

Ralph, F. M., Iacobellis, S., Neiman, P., Cordeira, J., Spackman, J., Waliser, D., Wick, G., White, A., & Fairall, C. (2017). Dropsonde observations of total integrated water vapor transport within north pacific atmospheric rivers. *Journal of Hydrometeorology*, *18*(9), 2577–2596.

Ralph, F. M., Rutz, J. J., Cordeira, J. M., Dettinger, M., Anderson, M., Reynolds, D., Schick, L. J., & Smallcomb, C. (2019). A scale to characterize the strength and impacts of atmospheric rivers. *Bulletin of the American Meteorological Society*, *100*, 269–289. https://doi.org/10.1175/bams-d-18-0023.1

Ramos, A. M., Trigo, R. M., & Liberato, M. L. R. (2014). A ranking of high-resolution daily precipitation extreme events for the iberian peninsula. *Atmospheric Science Letters*, n/a–n/a. https://doi.org/10.1002/asl2.507

Ramos, A. M., Trigo, R. M., & Liberato, M. L. R. (2016). Ranking of multi-day extreme precipitation events over the iberian peninsula. *International Journal of Climatology*, *37*, 607–620. https://doi.org/10.1002/joc.4726

Ramos, A. M., Trigo, R. M., Liberato, M. L. R., & Tomé, R. (2015). Daily precipitation extreme events in the iberian peninsula and its association with atmospheric rivers*. *Journal of Hydrometeorology*, *16*, 579–597. https://doi.org/10.1175/jhm-d-14-0103.1

Ruti, P. M., Somot, S., Giorgi, F., Dubois, C., Flaounas, E., Obermann, A., Dell'Aquila, A., Pisacane, G., Harzallah, A., Lombardi, E., et al. (2016). Med-cordex initiative for mediterranean climate studies. *Bulletin of the American Meteorological Society*, *97*(7), 1187–1208.

Slinskey, E. A., Loikith, P. C., Waliser, D. E., Guan, B., & Martin, A. (2020). A climatology of atmospheric rivers and associated precipitation for the seven us national climate assessment regions. *Journal of Hydrometeorology*, 1–55. https://doi.org/10.1175/jhm-d-20-0039.1

Soares, P. M., Cardoso, R. M., Lima, D. C., & Miranda, P. M. (2017). Future precipitation in portugal: High-resolution projections using wrf model and euro-cordex multi-model ensembles. *Climate Dynamics*, *49*, 2503–2530.

Soares, P. M., Careto, J. A., Russo, A., & Lima, D. C. (2023). The future of iberian droughts: A deeper analysis based on multi-scenario and a multi-model ensemble approach. *Natural Hazards*, 1–28.

Society, A. M. (2017). Atmospheric river - glossary of meteorology. *Ametsoc.org*.

BIBLIOGRAPHY

Trigo, I. F. (2005). Climatology and interannual variability of storm-tracks in the euro-atlantic sector: A comparison between era-40 and ncep/ncar reanalyses. *Climate Dynamics*, *26*, 127–143. https://doi.org/10.1007/s00382-005-0065-9

Trigo, R. M., Varino, F., Ramos, A. M., Valente, M. A., ZÃªzere, J. L., Vaquero, J. M., Gouveia, C. M., & Russo, A. (2014). The record precipitation and flood event in iberia in december 1876: Description and synoptic analysis. *Frontiers in Earth Science*, *2*. https://doi.org/10.3389/feart.2014.00003

Vicente-Serrano, S. M., Trigo, R., López-Moreno, J., Liberato, M., Lorenzo-Lacruz, J., Beguería, S., Morán-Tejeda, E., & El Kenawy, A. (2011). Extreme winter precipitation in the iberian peninsula in 2010: Anomalies, driving mechanisms and future projections. *Climate Research*, *46*, 51–65. https://doi.org/10.3354/cr00977

Vicente-Serrano, S. M., Beguería, S., & López-Moreno, J. I. (2010). A multiscalar drought index sensitive to global warming: The standardized precipitation evapotranspiration index. *Journal of Climate*, *23*, 1696–1718. https://doi.org/10.1175/2009jcli2909.1

Wick, G. A., Neiman, P. J., Ralph, F. M., & Hamill, T. M. (2013). Evaluation of forecasts of the water vapor signature of atmospheric rivers in operational numerical weather prediction models. *Weather and Forecasting*, *28*, 1337–1352. https://doi.org/10.1175/waf-d-13-00025.1

Wolber & Alfy. (1999). Monotonic cubic spline interpolation. *Proceedings Computer Graphics International CGI-99*. https://doi.org/10.1109/cgi.1999.777953

Zêzere, J. L., Pereira, S., Tavares, A. O., Bateira, C., Trigo, R. M., Quaresma, I., Santos, P. P., Santos, M., & Verde, J. (2014). Disaster: A gis database on hydro-geomorphologic disasters in portugal. *Natural Hazards*, *72*, 503–532. https://doi.org/10.1007/s11069-013-1018-y

Zhu, Y., & Newell, R. E. (1998). A proposed algorithm for moisture fluxes from atmospheric rivers. *Monthly Weather Review*, *126*, 725–735. https://doi.org/10.1175/1520-0493(1998)126<0725:apafmf>2.0.co;2